ROTAVIRUS INDUCES INTERCELLULAR CALCIUM WAVES THROUGH ADP SIGNALING

Authors: Alexandra L. Chang-Graham[1], Jacob L. Perry[1], Melinda A. Engevik[2,3], Heather A. Danhof[1], Francesca J. Scribano[1], Kristen A. Engevik[1], Joel C. Nelson[1], Joseph S. Kellen[1], Alicia C. Strtak[1], Narayan P. Sastri[1], Satya P. Kunapuli[5], Mary K. Estes[1,4], James Versalovic[2,3], Robert A. Britton[1], Joseph M. Hyser[1]

[1]Department of Molecular Virology and Microbiology, Baylor College of Medicine
[2]Department of Pathology and Immunology, Baylor College of Medicine
[3]Department of Pathology, Texas Children's Hospital
[4]Department of Medicine, Gastroenterology and Hepatology, Baylor College of Medicine
[5]Sol Sherry Thrombosis Research Center, Lewis Katz School of Medicine, Temple University

Correspondence should be sent to:
Joseph M. Hyser
Alkek Center for Metagenomic and Microbiome Research
Department of Molecular Virology and Microbiology
MS: BCM385
Baylor College of Medicine
Houston, TX, 77303
PH: 713-798-4514
FAX: 713-798-3586
Joseph.Hyser@bcm.edu

Abstract

Rotavirus causes severe diarrheal disease in children worldwide. A hallmark of rotavirus infection is an increase in cytosolic calcium in infected small intestine epithelial cells. However, the underlying mechanism(s) of rotavirus-cell signaling remains incompletely characterized. Here we show that rotavirus-infected cells produce paracrine signals that manifest as intercellular calcium waves (ICWs); which are observed in both cell lines and human intestinal enteroids (HIEs). Rotavirus ICWs are caused by the release of extracellular adenosine diphosphate (ADP) that activates P2Y1 purinergic receptors on neighboring cells and are blocked by P2Y1 antagonists or CRISPR/Cas9 knockout of P2Y1. This paracrine purinergic signal is critical for rotavirus replication and diarrhea. Blocking the ICW signal reduces rotavirus replication; inhibits rotavirus-induced serotonin release and fluid secretion; and reduces diarrhea severity in neonatal mice. This is the first evidence that viruses exploit intercellular calcium waves to amplify diarrheal signaling; a finding which have broad implications for gastrointestinal physiology.

Introduction

Rotavirus (RV), a non-enveloped double-stranded RNA virus of the *Reoviridae* family, causes severe diarrhea and vomiting in children worldwide, responsible for ~258 million diarrhea episodes and ~128,000 deaths annually [1]. Though the pathways by which other enteric pathogens cause diarrhea are well-characterized, such as cholera toxin of *Vibrio cholerae*, the mechanisms of RV diarrhea are multifactorial and still not completely understood. RV infects the epithelial enterocytes and enteroendocrine cells at the tip and middle of villi in the small intestine. Notably, only a percentage of cells susceptible to RV are infected, and diarrhea occurs before the onset of histopathologic changes [2–5]. During infection, RV dysregulates host cell calcium (Ca^{2+}) signaling pathways to increase cytosolic Ca^{2+}, which is required for RV replication. The RV nonstructural protein 4 (NSP4) drives these changes in Ca^{2+} homeostasis as both an intracellular viral ion channel (*i.e.*, viroporin) in the endoplasmic reticulum and an extracellular enterotoxin that elicits a phospholipase-C-dependent increase in cytosolic Ca^{2+} [6–8]. These perturbations to host Ca^{2+} signaling are known to activate autophagy, disrupt the cytoskeleton and tight junctions, and trigger fluid secretion pathways [7,9–12].

A long-held hypothesis in how RV infection causes life-threatening diarrhea is that RV-infected cells release potent signaling molecules that can dysregulate neighboring, uninfected cells [4,13,14]. This premise is based on previous studies that have identified increases in candidate signaling molecules during RV infection, including enterotoxin NSP4, prostaglandins (PGE2), and nitric oxide (NO) [7,15–17]. In this model, enterotoxin NSP4 can bind to neighboring, uninfected enterocytes to activate Ca^{2+}-activated chloride channels and cause secretory diarrhea [18,19], and PGE2 and NO may further activate fluid secretion processes [20,21]. Dysregulation of neighboring enteroendocrine cells triggers the Ca^{2+}-dependent release of serotonin, which stimulates the enteric nervous system both to activate vomiting centers in the central nervous system and to activate secretory reflex pathways in the gastrointestinal (GI) tract [5,22]. Thus, this model of RV-

64 induced diarrhea addresses how limited infection at the middle-to-upper villi may cause
65 widespread dysregulation of host physiology and life-threatening disease.

66 Herein we demonstrate that RV-infected cells signal to uninfected cells via an extracellular
67 purinergic signaling pathway. This newly identified pathway is a dominant driver of observed RV
68 disease processes, including replication, upregulation of PGE2- and NO-producing enzymes,
69 serotonin secretion, fluid secretion, and diarrhea in a neonatal mouse model. Our findings provide
70 new insights into the mechanism(s) of viral diarrhea and gastrointestinal physiology.

Results

Low multiplicity infection reveals intercellular calcium waves

Previous studies have shown that RV significantly increases cytosolic Ca^{2+} during infection and disrupts host Ca^{2+}-dependent processes to cause disease [23–25]. We used African Green monkey kidney MA104 cells stably expressing the genetically-encoded calcium indicator (GECI) GCaMP5G or GCaMP6s to observe changes in cytosolic Ca^{2+} during RV infection using live-cell time-lapse epifluorescence imaging. We did not observe differences in response using either GECI in our studies and refer to them together as GCaMP hereafter (*data not shown*). We mock- or RV (strain SA114F)-infected MA104-GCaMP cells at a low multiplicity of infection (MOI 0.01) to distinguish Ca^{2+} changes in infected cells compared to neighboring, uninfected cells. RV-infected cells were identified using immunofluorescence (IF) staining for RV antigen after imaging, and these IF images were superimposed on the time-lapse movies (**Fig. 1A**). While mock-infected cells had minimal changes in GCaMP fluorescence, RV-infected cells exhibited large fluctuations in fluorescence, and thus increases in cytosolic Ca^{2+}, as discrete signaling events, consistent with previous findings [26]. These signaling events not only increased cytosolic Ca^{2+} in the RV antigen-positive cell, but we also observed successive increases in cytosolic Ca^{2+} in neighboring, uninfected cells over a time interval of 30 s (**Fig. 1A, Supplementary Video 1**). We quantified the Ca^{2+}-eliciting signal from infected to uninfected cells using a previously described criterion in which changes in normalized relative fluorescence greater than 5% constituted a "Ca^{2+} spike" [26]. We observed that with neighboring cells 5 (NB+5) and 10 (NB+10) cells away from the infected cell, the number and average magnitude of the RV-induced Ca^{2+} transients decreased with increasing distance from the infected cell (**Fig. 1B, blue and purple traces**). Quantification of the number and magnitude of Ca^{2+} spikes of the infected, the NB+5, and the NB+10 cells show a significant decrease with distance from the infected cell (**Fig. 1C,D**). Together, this data constitutes the first direct observation of a RV-infected cell signaling to surrounding uninfected cells and eliciting a Ca^{2+} signaling response.

Next we sought to confirm that the Ca^{2+} signaling in the neighboring cells was not due to RV infection undetected by our antibody staining. MA104-GCaMP cells were mock-inoculated or infected with a recombinant SA11 clone 3 strain containing an mRuby3 fluorescent reporter (SA11cl3-mRuby3) as described previously [26], at MOI 0.01 and imaged for ~3-22 hours post-infection (hpi), conditions we used throughout these studies unless noted otherwise. We found no increase in mRuby3 fluorescence in the mock-infected cells but a steep increase in fluorescence in RV-infected cells by hour 12 of imaging that correlated with increased Ca^{2+} signaling (**Fig. 1E, left and middle panels, Supplementary Video 2**). Importantly, the NB+3 cell also had robust Ca^{2+} signaling by hour 12, but the lack of increase in mRuby3 fluorescence demonstrated it was not infected (**Fig. 1E, right panel**). As before, there was a similar decrease in the number of Ca^{2+} spikes and average Ca^{2+} spike magnitude in the NB+3 and NB+5 cells that correlated with increasing distance from the infected cell (**Fig. 1 F, G**). These findings demonstrate that the Ca^{2+} signaling in the neighboring cell is not due to infection of that cell but is due to signals activated by a nearby RV-infected cell.

Since RV-induced changes in Ca^{2+} homeostasis are driven by NSP4, we next determined if knockdown of NSP4 would reduce the Ca^{2+} signals in infected and uninfected cells. Using RV (SA11cl3-mRuby3), we infected MA104-GCaMP-shRNA cells expressing NSP4-targeted shRNA or a non-targeted scrambled shRNA described previously [26]. RV infection of the MA104-GCaMP-shRNA cells with the NSP4-isogenic RV strain SA114F has previously been shown to decrease NSP4 expression by ~85% and significantly decrease Ca^{2+} signaling [26]. Here we observed that the Ca^{2+} signaling frequency and Ca^{2+} spike magnitudes were significantly decreased in the NSP4-targeted shRNA MA104-GCaMP cells, both in RV-infected cells and NB+3 and NB+5 uninfected cells (**Fig. 1H-J**). These results support that the RV-induced Ca^{2+} signal requires the expression of RV NSP4 and the dysregulation of host Ca^{2+} homeostasis in the infected cell.

ADP and the P2Y1 receptor mediate RV-induced intercellular calcium waves

The pattern of signaling observed between RV-infected cells to uninfected cells is a phenomenon called intercellular calcium waves (ICWs), in which increases in cytosolic Ca^{2+} occur in an expanding circular pattern from a central initiating cell [27–29]. Several molecules have been implicated in ICW propagation and may communicate via gap junctions or through paracrine signaling [29]. To test if the RV-induced ICWs propagated via gap junctions, we infected MA104-GCaMP cells and treated with DMSO vehicle or the gap junction blockers 18β-glycyrrhetinic acid and TAT-Gap19. There was no significant difference in the Ca^{2+} spikes in neighboring cells between the mock-, 18β-glycyrrhetinic acid-, or TAT-Gap19-treated cells, supporting that the RV-induced ICWs did not propagate *via* gap junctions (**Fig. 2A**). This finding was consistent with a negative dye-loading scratch assay (**Extended Data Fig. S1A**). Next we tested if the extracellular enterotoxin form of NSP4 may be the signaling molecule responsible for propagating the ICWs by treating RV-infected MA104-GCaMP cells with purified anti-NSP4 rabbit antisera (120-147) known to bind to the enterotoxin domain[30] or purified anti-NSP4 monoclonal antibody 622 that neutralizes eNSP4-mediated Ca^{2+} flux (**Fig. 2B**). Addition of purified M60, a non-neutralizing anti-VP7 monoclonal antibody, was used as a control [31]. We did not observe a significant reduction in Ca^{2+} spikes in the neighboring cells treated with anti-NSP4 antibodies, suggesting that enterotoxin NSP4 was not responsible for the RV-induced ICWs (**Fig. 2B, Supplementary Video 3**). Previous studies found increased PGE2 and NO during RV infection, and thus are potential mediators of the RV-induced ICWs [15–17]. However, adding PGE2 or the NO donor NOC-7 to MA104-GCaMP cells did not elicit a Ca^{2+} response, and thus these molecules cannot directly mediate the RV-induced ICWs (**Extended Data Fig. S1B-E**). Together this data supports that ICW propagation is mediated by a signaling molecule not previously identified in RV infection.

We then sought to determine if ATP, an important extracellular messenger for many cell types and a common mediator of ICW signaling, was the signaling molecule responsible for the RV-induced ICWs[29]. We mock- or RV (SA11cl3-mRuby3)-infected MA104-GCaMP cells and mock-treated or treated with apyrase, an enzyme that degrades the purines ATP and ADP, after

inoculation. Apyrase-treated wells showed a dramatic decrease in the area of Ca^{2+} signaling compared to untreated wells (**Fig. 2C, Supplementary Video 4**). With apyrase treatment, the Ca^{2+} signaling frequency and amplitude are decreased both in the RV-infected cell and in neighboring, uninfected cells (**Fig. 2D**). The number of Ca^{2+} spikes and the average Ca^{2+} spike magnitude are significantly decreased in RV-infected wells treated with apyrase (**Fig. 2E-F**). These results support that extracellular ATP/ADP are the signaling molecules responsible for propagating ICWs in RV infection.

Purinergic signaling, i.e nucleotides as extracellular signals, is a key signaling pathway in intestinal physiology and involves multiple receptor subtypes. Using qPCR, we found that MA104 cells showed greatest expression of the purinergic receptors P2X4, P2X6, P2Y1, P2Y2, and P2Y14 (**Fig. 2G**). Relative mRNA expression levels of purinergic receptors did not substantially change with RV infection (**Extended Data Fig. S2A**). We first tested the ligand-gated ion channel P2X4 and the Gq/11 protein-coupled receptors P2Y1 and P2Y2 as they are strongly activated by ATP or ADP, which are well known to mediate ICWs [29]. We treated RV(SA11cl3-mRuby3)-infected MA104-GCaMP cells with small molecule inhibitors of the receptors (Bx430 and 5BDBD for P2X4, BPTU for P2Y1, and AR-C 118925XX for P2Y2). The P2X4 inhibitors Bx430 and 5BDBD or the P2Y2 inhibitor AR-C 118925XX had no effect on RV-induced Ca^{2+} signaling. We found that the P2Y1 blocker BPTU significantly decreased Ca^{2+} spikes in both the RV-infected cell and in the NB+3 cells, and this decrease was dose-dependent (**Fig. 2H-I, Extended Data Fig. S2C, Supplementary Video 5**). Additionally, we tested the specificity of the pharmacological blockers BPTU and AR-C 118925XX for their intended targets, the P2Y1 and P2Y2 receptors respectively, which are strongly activated by ADP and ATP respectively. We observed that the P2Y1 inhibitor BPTU significantly reduced the Ca^{2+} response in MA104-GCaMP cells from ADP, but not when ATP was added (**Extended Data Fig. S2D**). Similarly, the P2Y2 inhibitor AR-C 118925XX significantly reduced the Ca^{2+} response from ATP, but not from ADP, supporting that these pharmacological inhibitors are specific for their targets (**Extended Data Fig. S2D**). Together

these results support that the RV-induced ICWs are mediated by the extracellular release of ADP from infected cells and activation of the P2Y1 receptor on neighboring, uninfected cells.

RV induces intercellular calcium waves in human intestinal enteroids

MA104 cells are a robust model system to study RV replication and form a simple flat epithelium that facilitates microscopy studies. However, they are neither human nor intestinal in origin. To determine if RV also causes ICWs in intestinal epithelial cells, we used jejunum-derived human intestinal enteroids (HIEs) stably expressing the GECI GCaMP6s (jHIE-GCaMP6s) [26]. HIEs are an *in vitro* model system grown from human intestinal epithelial stem cells, making them a non-cancerous, non-transformed *in vitro* model of small intestine epithelium [32]. Furthermore, HIEs recapitulate the different epithelial cell types and support RV infection and replication, making them a biologically relevant system to study the gastrointestinal epithelium and disease processes [33–35]. We infected jHIE-GCaMP6s monolayers with mock inoculum or the human RV strain Ito and imaged at 4 hpi (**Fig. 3A, Supplementary Video 6**). We observed ICWs in both mock- and RV-infected jHIE-GCaMP6s monolayers; however, the areas of Ca^{2+} signaling were typically larger and had greater frequency in the RV-infected monolayer. To verify infection, we fixed the monolayers at 24 hpi, immunostained for RV antigen, and observed positive staining in the RV-infected monolayers (**Fig. 3B**). These observations support that ICWs occur under basal conditions in human intestinal epithelial cell models, but infection with RV increases the size of the ICWs.

Next, we investigated the mechanism of action of the RV-induced ICWs in the HIEs. To test gap junction transmission, we treated mock- or RV (Ito)-infected jHIE-GCaMP6s monolayers with DMSO vehicle, the glycyrrhetinic acid-derivative carbenoxolone (CBX), or the pannexin blocker [10]Panx. Since individual jHIE cells are much smaller and more mobile than MA104 cells, we were unable to perform single-cell analysis for these experiments. Instead we measured the GCaMP6s fluorescence over the whole field-of-view (FOV) (~455 μm^2). While we observed

statistically greater Ca^{2+} spikes in RV-infected than in mock-infected monolayers, we did not find a significant decrease in the number of Ca^{2+} spikes per FOV with CBX or ^{10}Panx treatment (**Fig. 2C**). Furthermore, the dye loading scratch assay was also negative in jHIE monolayers (**Extended Data Fig. S1A**). Adding PGE2 or NOC-7 to jHIE-GCaMP6s cells also did not elicit a Ca^{2+} response (**Extended Data Fig. S1F-I**). These results demonstrate that RV-induced ICWs do not occur through gap junctions or *via* PGE2/NO in HIEs.

We used qPCR to determine the purinergic receptor expression in jHIE monolayers and found that P2X4, P2Y1, and P2Y2 had the highest expression, similar to that of MA104 cells (**Fig. 2G, 3D**). The relative mRNA expression levels of purinergic receptors did not substantially change with RV (Ito) infection (**Extended Data Fig. S2B**). To test the involvement of the different purinergic receptors in ICWs, we mock- or RV (Ito)-infected jHIE-GCaMP6s monolayers and treated with DMSO vehicle, apyrase, BPTU, AR-C 118925XX, Bx430, or 5BDBD, and we found that apyrase and BPTU treatment decreased the Ca^{2+} signaling and amplitude in RV-treated monolayers (**Fig. 3E, Supplementary Video 7**). Quantification verified a significant decrease in the number of Ca^{2+} spikes/FOV and average Ca^{2+} spike magnitude with apyrase or BPTU treatment compared to the DMSO vehicle control in the RV-infected monolayers (**Fig. 3F,G**). Interestingly, BPTU and apyrase treatment also reduced the number of Ca^{2+} spikes in mock-inoculated monolayers (**Fig. 3F**), which indicates that jHIEs commonly utilize purinergic receptor-induced Ca^{2+} signaling under basal conditions and this is exploited during RV infection.

Since jHIEs are human-derived cultures, genetic variation may influence whether RV-infection can cause ICWs. We created an additional jHIE-GCaMP6s line derived from a different patient, and then mock- and RV-infected these jHIE-GCaMP6s monolayers and treated with a panel of P2Y1 receptor blockers (BPTU, MRS2179, MRS2279, and MRS2500). We found that all of the P2Y1 blockers significantly decreased the number of Ca^{2+} spike/FOV and average Ca^{2+} spike magnitude when compared to DMSO vehicle control for both the mock- or RV-infected

monolayers (**Fig. 3H,I**). Together, this data supports that RV-induced ICWs in intestinal epithelial cells occur by extracellular ADP signaling and the P2Y1 receptor, the same as in MA104 cells.

CRISPR/Cas9 P2Y1 receptor knockout reduces intercellular calcium waves

Pharmacological studies of purinergic receptors have found that different receptors have distinct affinities for nucleotide binding, with the P2Y1 receptor having greater activation with ADP than with ATP [36]. This suggests that ADP mediates the ICWs in RV infection, which is also consistent with studies that have found that RV-infected cells have reduced cytoplasmic concentrations of ATP [37]. To test whether ADP is the signaling molecule of the ICWs, we infected MA104-GCaMP cells with RV (SA114F) and then treated with apyrase grade VI, which has a high ATPase/ADPase activity ratio, or apyrase grade VII, which has a low ATPase/ADPase activity ratio. Treatment with apyrase grade VII, but not grade VI, significantly decreased the number of Ca^{2+} spikes and the spike magnitude in RV-infected wells, supporting that ADP is the signaling molecule in RV-induced ICWs (**Fig. 4A,B**). To further test that the P2Y1 receptor is required for RV-induced Ca^{2+} waves, we genetically knocked out the P2Y1 receptor in MA104-GCaMP cells using lentivirus encoding CRISPR/Cas9 with small-guide RNAs targeted for the P2Y1 receptor gene (MA104-GCaMP-P2Y1ko). Genotyping analysis revealed several mutations in the sequence downstream of the guide RNA in 3 clonal populations of cells (**Extended Data Fig. S3A,B**). To test the P2Y1 knockout phenotype, we added ADP to parental and MA104-GCaMP-P2Y1ko cells and found a significantly decreased Ca^{2+} response in the knockout cells compared to the parental GECI line, consistent with a lack of P2Y1 receptor function (**Fig. 4C**).

Next, we sought to determine if knockout of the P2Y1 receptor would also prevent ICWs during RV infection. We mock- or RV (SA114F)-infected MA104-GCaMP (parental) or MA104-GCaMP-P2Y1ko cells. Fixing and immunostaining for RV antigen at 24 hpi showed positive staining for RV in parental and P2Y1 knockout cells confirming that the P2Y1 knockout did not prevent infection (**Fig. 4D**). In the P2Y1 knockout cells, there was a decrease in Ca^{2+} signaling,

Ca^{2+} spikes, and average Ca^{2+} spike magnitude in the NB+3 and NB+5 cells compared with the parental, though not in the RV-infected cell (**Fig. 4E-G, Supplementary Video 8**). Additional treatment of apyrase VII to the P2Y1 knockout cells only modestly decreased the Ca^{2+} spikes in neighboring cells (**Fig. 4G**).

Similarly, we tested the effect of genetic knockout of the P2Y1 receptor on ICWs in RV-infected jHIEs (jHIE-GCaMP6s-P2Y1ko). Genotyping analysis revealed two P2Y1 knockout enteroid populations comprising of an insertional mutation and a deletion in the sequence downstream of the guide RNA (**Extended Data Fig. S3C,D**). Phenotypic knockout was confirmed by a reduced Ca^{2+} response to ADP in jHIE-GCaMP6s-P2Y1ko enteroids compared to parental enteroids (**Fig. 5A**). For these studies we also created an additional jHIE-GCaMP6s enteroid line with CRISPR/Cas9 knockout of the P2Y2 receptor (jHIE-GCaMP6s-P2Y2ko). Genotyping analysis of the P2Y2ko enteroids detected two alleles with deletion mutations downstream of the guide RNA sequence (**Extended Data Fig. S4A,B**). To test the P2Y2 knockout phenotype, we added non-hydrolyzable ATP-γS to parental and P2Y2ko enteroids and found a significantly decreased Ca^{2+} response in the P2Y2ko jHIEs (**Fig. 5B**). Immunostaining the jHIE monolayers for RV antigen at 24 hpi showed positive staining for RV in parental, P2Y1ko, and P2Y2ko enteroids, demonstrating RV infection still occurred (**Fig. 5C,D**). Mock- or RV (Ito)-infection of the parental, jHIE-GCaMP6s-P2Y1ko, or jHIE-GCaMP6s-P2Y2ko resulted in significantly less Ca^{2+} signaling, Ca^{2+} spikes/FOV, and smaller average Ca^{2+} spike magnitude in the P2Y1 knockout jHIEs, but not in P2Y2 knockout jHIEs (**Fig. 5E-G, Supplementary Video 9**). Interestingly, there was also significantly fewer Ca^{2+} spikes/FOV and average Ca^{2+} spike magnitude in the P2Y1 KO enteroids compared to parental or P2Y2 knockout enteroids in mock-inoculation (**Fig. 5F,G**). Together, this data supports that ADP and the P2Y1 receptor mediate the ICWs in RV infection and reduce basal ICW signaling.

Purinergic signaling increases RV replication and expression of IL-1α, iNOS, and COX2

278 Previous studies have found that extracellular ATP reduces the replication of several
279 viruses through activation of P2X7 receptors, which specifically bind ATP [38,39]. Less is known
280 about the role of ADP in cellular signaling or its effects on viral infection and replication. We first
281 tested the effect of purinergic blockers on RV replication. New infectious yield from RV (SA114F)-
282 infected MA104 cells was decreased when treating cells with apyrase or BPTU after inoculation,
283 and no significant decrease was observed when adding AR-C 118925XX, Bx430, 5BDBD, or the
284 non-selective P2 receptor antagonists suramin and PPADS (**Fig. 6A**). Furthermore, RV infectious
285 yield was also reduced from RV (SA11cl3-mRuby)-infected MA104-GCaMP-P2Y1ko cells
286 compared to parental MA104-GCaMP cells (**Fig. 6B**). These results support that blocking ADP
287 signaling and the P2Y1 receptor decreases RV replication.

288 Extracellular ATP is also known to have pro-inflammatory functions and activate
289 components of the innate immune system such as macrophages [40,41]. Previous studies have
290 found that RV increases expression and release of the inflammatory cytokine interleukin-1α (IL-
291 1α), which is highly expressed in epithelial cells [42,43]. Furthermore, strong cytosolic Ca^{2+} agonists
292 can induce the secretion of IL-1α independent of inflammasome activation [44]. To determine if RV-
293 induced ICWs increase IL-1α, we mock- or RV (Ito)-infected jHIE monolayers and treated with
294 apyrase or BPTU. RV infection significantly increased *IL-1α* expression over mock infection, and
295 treatment with apyrase or BPTU inhibited this increase (**Fig. 6C**). This finding supports that RV-
296 induced ICWs and ADP signaling increases *IL-1α* expression and thus mediates the inflammatory
297 response from HIEs.

298 Since increased PGE2 and NO have been found during RV infection, we also investigated
299 if RV-induced ICWs could stimulate their production [15–17]. Previous studies have found that
300 purinergic signaling stimulates cyclooxygenase-2 (*COX2*) expression and PGE2 release from
301 Caco-2 and rat-derived IEC-6 cell lines and can also activate inducible nitric oxide synthase
302 (*iNOS)* expression and nitric oxide production [45,46]. To test the role of ADP signaling, we mock- or
303 RV (Ito)-infected jHIE monolayers and treated with apyrase or BPTU. RV infection significantly

304 increased both *COX2* and *iNOS* expression over mock-infection, and treatment with apyrase or
305 BPTU inhibited this increase (**Fig. 6D-E**). These findings suggest that RV-induced ICWs and ADP
306 signaling increase the expression of *COX2* and *iNOS* and thus potentially drive the increased
307 PGE2 and NO observed in RV infections.
308
309 *Blocking purinergic signaling reduces serotonin and fluid secretion*
310 RV infection causes a multifactorial secretory diarrhea, and two-thirds of the fluid secretion
311 can be attributed to activation of the enteric nervous system (ENS) [5]. Previous studies have found
312 that RV infection can stimulate the release of serotonin from enterochromaffin cells to activate the
313 ENS and blocking serotonin decreases diarrhea, making serotonin release a key mechanism for
314 RV-induced diarrhea [22,47]. To determine if RV-induced ADP signaling could stimulate serotonin
315 secretion, we mock- or RV (Ito)-infected jHIE monolayers and treated with DMSO vehicle,
316 apyrase, or BPTU. After 24 hr, we found significantly increased serotonin in the supernatant of
317 RV-infected jHIE monolayers compared to mock-infection, which was significantly inhibited by
318 treatment with apyrase or BPTU (**Fig. 6F**). Furthermore, treatment of RV-infected monolayers
319 with ω-agatoxin, a P-type voltage-gated Ca^{2+} channel blocker, also significantly inhibited
320 serotonin levels, supporting that the measured serotonin was from cellular release rather than cell
321 death (**Fig. 6F**). We found similar results when infecting jHIE transwells, a more polarized model
322 of epithelium, with RV. Treatment with BPTU significantly decreased serotonin measured in both
323 the apical and basolateral compartments compared with DMSO vehicle and overall a greater
324 concentration of serotonin secreted basally (**Fig. 6G**). This data support that ADP signaling
325 stimulates serotonin secretion during RV infection.
326 RV infection also activates secretory pathways in epithelial cells through the stimulation
327 of chloride secretion which drives paracellular movement of water. We tested whether RV-induced
328 ADP signaling was important for RV-induced epithelial fluid secretion using the enteroid swelling
329 assay, in which an increase in fluid secretion causes an increase in the internal lumen of three-

dimensional (3D) enteroid cultures [33,48]. We mock- or RV-infected 3D jHIE-GCaMP6s enteroids, treated with DMSO vehicle or BPTU, and found that BPTU treatment significantly decreased the percentage of swelling in RV-infected enteroids (**Fig. 6H, Supplementary Video 10**). This result supports that ADP signaling stimulates epithelial fluid secretion in RV infection.

Finally, we determined whether inhibition of the P2Y1 receptor would attenuate RV-induced diarrhea in a neonatal mouse model. BPTU consistently had the most potent inhibition of Ca^{2+} spikes and average Ca^{2+} spike magnitude in HIEs (**Fig. 3H,I**). We tested a drug treatment model in which 6 to 8-day-old pups were orally gavaged with rhesus RV (RRV) and then gavaged with BPTU or vehicle control on days 1-4 post-infection. Stools were assessed each day and watery, mucus, yellow stools were indicators of diarrhea. Peak diarrhea occurred at 2 dpi in both DMSO- and BPTU-treated pups, but the percentage of pups with diarrhea decreased significantly on 4 dpi (**Fig. 6I**). Pups treated with BPTU also had significantly less severe diarrhea as measured by their mean diarrhea score (**Fig. 6J**). Furthermore, the intestinal cross-sections from the duodenum, jejunum, and ileum of RV-infected pups treated with DMSO or BPTU are relatively similar with no histopathological features at 5 dpi (**Fig. 6K**). These studies support that blocking the P2Y1 receptor decreased diarrhea severity and caused diarrhea to resolve more quickly than the untreated animals.

We next tested whether treatment with a water-soluble small molecule P2Y1 receptor blocker, MRS2500, would similarly attenuate RV diarrhea. In these studies, we found there was a decreased percentage of diarrhea in pups gavaged with MRS2500 on 1 dpi compared to pups treated with normal saline, but on other dpi, there were similar percentages of diarrhea (**Extended Data Fig. S5A**). Pups treated with MRS2500 also had significantly less severe diarrhea on 1 dpi and 3 dpi than pups treated with saline (**Extended Data Fig. S5B**). These results further support that inhibition of P2Y1 decreases RV diarrhea severity.

Finally, we used a neonatal mouse model of RV diarrhea using a constitutive knockout of the P2Y1 receptor [49]. Interestingly, RRV infection of the P2Y1 knockout mice did not abolish RV-

induced diarrhea (**Extended Data Fig. S5C,D**). We measured the purinergic receptor expression in neonatal jejunum epithelium in a C57Bl/6 background and in the P2Y1 knockout mice. With the exception of P2Y1 transcripts, we found similar relative expression levels of P2X4, P2Y2, P2Y6, and P2Y13 in both mice (**Extended Data Fig. S5E,F**). P2Y2 and P2Y6 are also Gq protein-coupled receptors and may be activated in RV infection of neonatal mice.

Discussion

The current model of RV pathogenesis proposes that paracrine signaling from RV-infected cells dysregulates surrounding uninfected cells and contributes to life-threatening diarrhea and/or vomiting. Previous studies have established that RV elevates cytosolic calcium during infection and increases paracrine signaling molecules such as eNSP4, PGE2, and NO, but signaling from RV-infected cells to uninfected cells had not been determined [7,16,17]. Thus, the primary goal of this study was to investigate the role of intercellular signaling during RV infection and to identify the signaling mechanisms involved. Using GECI-expressing cell lines and HIEs, we used long-term live-cell fluorescence imaging to detect signaling between infected and uninfected cells. Our work describes the first direct observation of ICWs originating from RV-infected cells and has provided experimental proof the widely held paracrine signaling model. However, the discovery of ADP signaling as both the paracrine signal and the most dominant Ca^{2+} signal observed in RV infection is paradigm-shifting. Extracellular purine signaling is a well-conserved communication system found in single-celled bacteria and protozoa as well as plants and higher order eukaryotes [50]. RV is the first virus observed to activate ICWs and furthermore this signaling is mediated by ADP, rather than ATP, and the ADP-selective P2Y1 receptor. RV exploits ADP signaling in host cells to benefit its replication, but this signaling also leads to increased fluid and serotonin secretion that are hallmarks of RV disease. Furthermore, we found that treatment of neonatal mice with a small molecule P2Y1 receptor blocker was able to attenuate RV diarrhea, underlining that activation of purinergic signaling is biologically relevant to RV disease. Activating ICWs and ADP

382 signaling may be a common strategy for enteric viruses to amplify dysregulation of host cells, and
383 thus targeting the P2Y1 receptor may be an effective host-directed approach to treating viral
384 diarrhea.

385 Additionally, ICWs and extracellular ADP signaling may be a broadly important form of
386 communication in the gastrointestinal epithelium. Basal ICWs in jHIEs were reduced when treated
387 with apyrase and P2Y1 blockers and P2Y1 receptor knockout enteroids had significantly reduced
388 Ca^{2+} signaling. Since ATP-mediated ICWs are activated in wound healing responses [56,57], tonic
389 purinergic signaling may also be important for epithelial-to-epithelial cell communication and
390 maintaining the integrity of the epithelial barrier. Purinergic signaling is well known to regulate
391 responses to injury and restitution by mediating the innate immune system [41]. We speculate that
392 basal, ADP-based ICWs may have a role in the balance of pro- and anti-inflammatory signaling
393 from the epithelium. Furthermore, extracellular ATP signaling in the GI tract stimulates epithelial
394 ion transport [58], suggesting a role for basal ICWs to stimulate fluid secretion and hydrate the
395 mucus layer. Finally, ADP-driven ICWs may mediate communication between the epithelium to
396 the enteric nervous system directly or signal to the lamina propria and endothelium as part of
397 tissue-level homeostasis. As the epithelium is the primary interface between the environment and
398 the host, understanding how it coordinates and communicates is critical for developing
399 therapeutics when it becomes dysregulated in disease states. Together, these studies identify the
400 signaling compound that elicits a paracrine signal involved in diarrhea and/or vomiting responses.
401 Our studies demonstrated that reduction of ADP signaling and ICWs reduces many known
402 aspects of RV disease including serotonin release, epithelial fluid secretion, and diarrhea in a
403 neonatal mouse model. Since ICWs and ADP signaling are involved in RV disease processes,
404 targeting the P2Y1 receptor may be an effective approach to treating viral diarrhea. This is the
405 first known example that viruses can exploit purinergic signaling and ICWs, and this may be a
406 common strategy for enteric viruses to amplify dysregulation of pathophysiological signaling
407 important for diarrhea.
408

Methods

Cells and rotaviruses. MA104 cells (African green monkey kidney cells) and HEK293T cells (ATCC CRL-3216) were cultured in high glucose DMEM supplemented with 10% fetal bovine serum (FBS) and Antibiotic/Antimycotic (Invitrogen) at 37°C in 5% CO_2. The rotavirus human strain Ito, used for all human intestinal enteroid infections, was prepared as previously described [33]. Rotavirus strains SA114F and RRV were produced from in-house stocks. Recombinant and SA11 clone 3-mRuby3 was produced previously [26]. All viruses were propagated in MA104 cells in serum-free DMEM supplemented with 1 μg/mL Worthington's Trypsin, and after harvest stocks were subjected to three freeze/thaw cycles and activated with 10 μg/mL Worthington's Trypsin for 30 min at 37 °C prior to use.

Rotavirus diarrhea mouse model. P2Y1-null mice were gifts from S. Kunapali (Temple University, Philadelphia, PA) used previously [49]. P2Y1-null mice were genotyped with primers listed in **Extended Data Table 1** using ear notch lysates performed on whole genomic DNA prepared using DirectPCR (Viagen) with Proteinase K (Qiagen) according to manufacturer's instructions. C57Bl/6J dams with natural litters (purchased from Center for Comparative Medicine, Baylor College of Medicine) were used and housed in standard cages with food and water provided *ad libitum*. Mouse pups, both male and female at natural ratios, were housed with their dam throughout the experiment. Animal experiments were approved by the Baylor College of Medicine Institutional Animal Care and Use Committee (IACUC), approved protocol AN-6903. All experiments were performed in accordance with the recommendations in the Guide for the Care and Use of Laboratory Animals of the National Institutes of Health.

Six- or seven-day-old mouse pups were orally gavaged with 1.5 x 10^5 PFU/mL of Rhesus rotavirus, a dosage sufficient to cause diarrhea in 100% of pups. The inoculum was mixed with sterile-filtered green food dye (3% by volume) for visualization of the gavage. For BPTU

experiments, pups were orally gavaged with BPTU (4 mg/kg) (4 cages, n = 30 pups) or an equivalent volume of DMSO vehicle control (4 cages, n = 26 pups) suspended in pharmaceutical grade corn oil on days 1-4 post-infection. For MRS2500 experiments, pups were orally gavaged with MRS2500 (4 mg/kg) (5 cages, n = 30 pups) or an equivalent volume of saline control (4 cages, n = 21 pups) suspended in pharmaceutical grade normal saline on days 1-4 post-infection. Four cages with a total of 30 pups were used in P2Y1$^{-/-}$ experiments. Each day, mouse pups were gently palpated on the abdomen to express and visualize feces. Stools were assessed on a scale between 1-4 for volume, color, and consistency as described previously [7], an average score of ≥2 was considered diarrhea. For scoring consistency, select experiments were scored by an observer blinded to experimental condition. Percentage of pups with diarrhea was calculated as the number of stools with a diarrhea score ≥ 2 divided by the number of stools collected per cage per day. Pups from which a stool sample could not be collected on that day were not counted for percent diarrhea or mean diarrhea severity calculations.

Chemicals. BPTU, AR-C 118925XX, Bx430, 5-BDBD, MRS2179, MRS2279, MRS2500, 10-Panx, suramin, TAT-Gap19, PPADS (Pyridoxalphosphate-6-azophenyl-2',4'-disulfonic acid), NOC-7, prostaglandin E2, and ω-agatoxin were purchased from Tocris Bioscience. Apyrase grade VI (catalog no. A6410) and apyrase grade VII (catalog no. A6535) were purchased from Sigma-Aldrich. 18β-glycyrrhetinic acid and carbenoxolone were purchased from Santa Cruz Biotechnology.

Antibodies. To detect RV by IF, we used rabbit anti-RV strain Alabama [10] (1:80,000) and the secondary antibody donkey anti-rabbit AlexaFluor 568 (Invitrogen) (1:2000). For eNSP4-blocking assays, we used purified anti-NSP4 rabbit antisera (120-147)[30], purified anti-NSP4 monoclonal antibody 622 (data in preparation), and purified M60, a non-neutralizing anti-VP7 monoclonal

antibody, was used as a control [31]. Equal concentrations of antibody, estimated using protein OD280, were added to RV-infected wells after inoculation.

Calcium indicator lentiviruses, cell lines, and enteroids. GCaMP5G (Addgene plasmid #31788), GCaMP6s (Addgene plasmid #40753), and G-CEPIA1er (Addgene plasmid #105012) were cloned into pLVX-Puro. RGECO1.2 (Addgene plasmid #45494), R-CEPIA1er (Addgene plasmid #58216), and GCaMP6s were cloned into pLVX-IRES-Hygro. Lentivirus vectors for the GECI constructs were packaged in HEK293T cells as previously described[59] or produced commercially (Cyagen Biosciences, Inc.). MA104-GCaMP5G, MA104-GCaMP5G/RCEPIAer, MA104-RGECO1/GCEPIAer, and the MA104-GCaMP6s-shRNA lines and jHIE-CaMP6s enteroids (from patient J3) were generated as previously described [26,59]. Both MA104-GCaMP5G and MA104-GCaMP6s cells were used in these studies; we observed no difference in calcium responses with these two indicators and thus refer to both as MA104-GCaMP. Jejunum human intestinal enteroids from patient J2 expressing GCaMP6s (in pLVX-IRES-Hygro) were created using lentivirus transduction as described previously and grown in high Wnt3a CMGF+ with 50 µg/mL hygromycin B for selection [60].

CRISPR/Cas9 KO cell lines and enteroids. Lentivirus constructs in pLentiCRISPRv2 vectors were purchased from GenScript Biotech Corp (USA) and were packaged in HEK293T cells as previously described [59]. The CRISPR/Cas9-expression vectors encode a puromycin-resistance gene for drug selection. The following small guide RNAs were used: P2Y1-sg1 CTACAGCATGTGCACGACCG and P2Y2-sg1 TTTGTCACCACCAGCGCGCG. MA104-GCaMP6s cells (pLVX-IRES-Hygro) were transduced with the P2Y1 CRISPR/Cas9-expressing construct and at 72 hrs post-transduction the cells were passaged in the presence of 50 µg/mL hygromycin B and 10 µg/mL puromycin to select for co-expression of GCaMP6s and CRISPR/Cas9. The patient J2-derived jHIE-GCaMP6s(hygro) enteroids described above were

transduced with the CRISPR/Cas9-expressing constructs to make two separate enteroid lines and grown with 50 μg/mL hygromycin B and 1 μg/mL puromycin to select for co-expression of GCaMP6s and CRISPR/Cas9.

Genotyping was performed on whole genomic DNA prepared using DirectPCR (Viagen) with Proteinase K (Qiagen) according to manufacturer's instructions. Genomic DNA was a template to PCR amplify a region surrounding the P2Y1 or P2Y2 sgRNA-target sites using primers listed in **Extended Data Table 1**. PCR products were cloned into the pMiniT2.0 vector using the NEB PCR Cloning Kit (New England Biolabs). Five clones for P2Y1ko HIEs and five clones for P2Y2ko HIEs were picked and sequenced to determine the repertoire of alleles present in the HIE cultures. Sanger sequencing was performed by GENEWIZ (USA).

Phenotypic knockout was tested through measurement of relative GFP fluorescence increase after addition of 1 nM ADP for MA104-GCaMP6s-P2Y1ko cells, 10 nM ADP for (J2)HIE-GCaMP6s-P2Y1ko enteroids and 10 μM ATP-γS for (J2)HIE-GCaMP6s-P2Y2ko enteroids compared to parental (J2)HIE-GCaMP6s-P2Y2ko enteroids. Experiments were performed at least 3 times with n ≥ 25 cells per experiment analyzed.

Establishment of HIE cultures. The human intestinal enteroid (HIE) cultures used in this study were generated previously and deposited into the Texas Medical Center Digestive Diseases Center (TMC-DDC) Gastrointestinal Experimental Model Systems (GEMS) Core [32,33]. We used jejunal HIEs from patients J2 and J3, both adult females, obtained from the GEMS core. Complete media with and without growth factors (CMGF+ and CMGF-, respectively), differentiation media, high Wnt3a CMGF+ (hW-CMGF+), and a Fluorobrite-DMEM based differentiation media (FB-Diff) were prepared as previously described [26,32,33,60]. HIEs were grown in phenol red-free, growth factor-reduced Matrigel (Corning). HIE monolayers were prepared from three-dimensional cultures and seeded into optical-bottom 10-well Cellview chamber slides coated with dilute

collagen IV (Sigma) as described previously [61,62]. After 24 hr in CMGF+ and 10 μM Y-27632 Rock inhibitor, differentiation medium was used and changed every day for 4-5 days.

Microscopy and image analysis. For calcium imaging, MA104 cells and HIEs were imaged with a widefield epifluorescence Nikon TiE inverted microscope using a SPECTRAX LED light source (Lumencor) and either a 20x Plan Fluor (NA 0.45) phase contrast or a 20X Plan Apo (NA 0.75) differential interference contrast (DIC) objective. Fluorescence and transmitted light images were recorded using an ORCA-Flash 4.0 sCMOS camera (Hamamatsu), and Nikon Elements Advanced Research v4.5 software was used for multipoint position selection, data acquisition, and image analysis. Images were read-noise subtracted using an average of 10 no-light acquisitions of the camera. Single cells were selected as Regions of Interest (ROI) and fluorescence intensity measured for the experiment. The fluorescence intensity of the whole field-of-view was measured for HIE monolayers. Fluorescence intensity values were exported to Microsoft Excel and normalized to the baseline fluorescence. The number and magnitude of Ca^{2+} spikes were calculated as described previously [26]. Ca^{2+} signals with a ΔF magnitude of > 5% were counted as Ca^{2+} spikes. Average relative fluorescence increase in Ca^{2+} spike magnitude was calculated from the highest 50 Ca^{2+} spikes per cell or per field of view for HIE monolayers.

Calcium imaging.

MA104-GECI cells. Fluorobrite DMEM supplemented with 15mM HEPES, 1X sodium pyruvate, 1X Glutamax, and 1X non-essential amino acids (Invitrogen) was used for fluorescence Ca^{2+} imaging (FB-Plus). Confluent monolayers of MA104-GCaMP cells in gridded 8-well chamber slides (ibidi) were mock- or RV-infected in FBS-free media for 1 hr at the indicated multiplicity of infection (MOI). The inoculum was removed and replaced with FB-Plus, and for experiments where noted, with DMSO vehicle or drugs at indicated concentrations. For experiments with gap junction blockers, either 30 μM 18β-glycyrrhetinic acid (18β-gly) or 50 μM TAT-Gap19 (Gap19)

was added. For experiments with apyrase, either 10 U/mL of apyrase VI, 10 U/mL of apyrase VII, or a mixture of 5 U/mL of apyrase VI and 5 U/mL of apyrase VII was added. For experiments with purinergic receptor blockers, 10 μM BPTU, 10 μM AR-C 118925XX, 10 μM Bx430, or 10 μM 5-BDBD was used or otherwise noted. The slide was mounted into an Okolab microscope stage-top incubation chamber equilibrated to 37°C with a humidified 5% CO_2 atmosphere. In each experiment, 3-5 positions per well were selected and imaged every 1 minute for ~3-22 hours post infection. Each imaging experiment was performed at least three times independently, and data shown are representative of 1-3 experiments combined.

GECI HIEs. For RV infection in monolayers, jHIE-GCaMP6s monolayers were washed once with CMGF- and treated with an inoculum of 50 μL CMGF- plus 30 μL MA104 cell lysate or RV (Ito) and incubated at 37°C and 5% CO_2 for 2 hr. Then inoculum was removed, and monolayers were washed once with FB-Diff before adding FB-Diff with DMSO or drugs at indicated concentrations. For experiments with apyrase, a mixture of 50 U/mL of apyrase VI and 50 U/mL of apyrase VII was added. For experiments with purinergic receptor blockers, 10 μM BPTU, 10 μM AR-C 118925XX, 10 μM Bx430, 10 μM 5-BDBD, 10 μM MRS2179, 10 μM MRS2279, or 10 μM MRS2500 was used. Monolayers were transferred to the stage-top incubator for imaging with 4 fields of view chosen per well and imaged every minute for ~7-22 hours post-infection. Each imaging experiment was performed at least three times independently, and data shown are representative of all replicates combined.

Enteroid swelling assay. Jejunum HIEs were split and grown in hW-CMGF+ for 2 days followed by differentiation medium for 1 day. jHIEs were gently washed using ice cold 1XPBS and suspended in inoculum of 50 μL MA104 cell lysate or RV (Ito) diluted with 150 μL CMGF- and incubated for 1 hr. Then HIEs were washed, resuspended in 25% Matrigel diluted in FB-Diff (with DMSO vehicle or BPTU) and pipetted onto 8-well chamber slides (Matek) pre-coated with

Matrigel. Imaging positions were chosen so that between 30-50 enteroids were selected per experimental condition. Enteroids were imaged using the stage-top incubator with transmitted light and GFP fluorescence every 2-3 minutes for ~18 hrs. Swelling was determined by measuring the cross-sectional area of the internal lumen at the beginning of the run compared to the time point of maximum swelling and calculating the percent increase. Area measurements were determined using the Nikon Elements AR v4.5 software. Experiments were performed three times independently, and data shown are representative of all replicates combined, n ≥ 68 HIEs per condition.

Dye loading scratch assay. Lucifer Yellow in Hank's Buffered Salt Solution (HBSS) (1mg/mL) or Rhodamine 123 in H_2O (1mg/mL) was diluted 1:100 in FB-Plus and added to MA104 or jHIE cell monolayers. Monolayers were scraped with a 26 *g* needle and incubated for 5 min at room temperature. Monolayers were then washed 3 times with FB-Plus and imaged. Images representative of each experiment were performed in triplicate.

Immunofluorescence. MA104 cells and HIEs were fixed using the Cytofix/Cytoperm kit (BD Biosciences) according to manufacturer instructions. Primary antibodies were diluted in 1X Perm/Wash overnight at 4°C. The next day, the cells were washed three times with 1X Perm/Wash solution and then incubated with corresponding secondary antibodies for 1 hr at room temperature. Nuclei were stained with NucBlue Fixed Cell Stain (Life Technologies) for 5 min at room temperature and washed with 1X PBS for imaging. Experiments were performed three times independently.

Fluorescence focus assay. Fluorescence focus assays (FFA) were performed as described previously with the following modifications [11]. After inoculation with RV, MA104 cells were treated with DMSO, 10U/mL apyrase, 10 μM BPTU, 10 μM AR-C 118925XX, 20 μM Bx430, 20 μM 5-

BDBD, 300 μM suramin, or 10 μM PPADS. Then, cells and media at 24 hpi were freeze-thawed three times and then with activated with 10 μg/mL Worthington's Trypsin for 30 min at 37 °C prior to use. Ten-fold dilutions were used to inoculate MA104 monolayers in 96-well plates for 1 hr and cells were fixed at 20 hpi with ice-cold methanol for ~20 min at 4°C, then washed 3 times with 1X phosphate buffered solution (PBS). Primary rabbit anti-rotavirus antisera[10] was used at 1:100,000 and incubated overnight at 4°C. Monolayers were washed 3x with 1XPBS and then incubated with secondary antibody donkey anti-rabbit AlexaFluor 488 (1:2000) for 1 hr at 37°C and then washed 3x with 1XPBS prior to imaging. FFA experiments were performed three times independently.

Plaque assay. Plaque assays were performed as described previously with the following modifications [63]. Briefly, MA104 cells were seeded and grown to confluency in 6 well plates. Wells were infected at 10-fold dilutions in duplicate for 1 hr and media replaced with an overlay of 1.2% Avicel in serum-free DMEM supplemented with DEAE dextran, and 1μg/mL Worthington's Trypsin, and, for indicated experiments, DMSO vehicle, apyrase, or purinergic receptor blocker drugs [64]. The cells were incubated at 37°C/5% CO_2 for 48-72 hrs before overlay was removed and cells stained with crystal violet to count plaques. Plaque assays of using MA104-GCaMP and MA104-GCaMP-P2Y1ko cells were performed three times independently, and data shown are representative of all replicates combined.

RNA extraction, reverse transcription, and quantitative PCR. Total RNA was extracted from HIE 96-well monolayers or MA104 cells grown to confluency in a 6-well plate using TRIzol reagent (Ambion). In RV-infection experiments, cells were harvested at 24 hpi. Total RNA was treated with Turbo DNase I (Ambion) and cDNA was generated from 250 ng RNA using the SensiFAST cDNA synthesis kit (Bioline). Quantitative PCR was performed using Fast SYBR Green (Life Technologies) with primers (**Extended Data Table 2**) and using the QuantStudio real time

thermocycler (Applied Biosciences). Target genes were normalized to the housekeeping gene ribosomal subunit 18s and relative expression was calculated using the ddCT method. Experiments were performed three times independently, and data shown are representative of all replicates combined. For *IL-1α*, *COX2*, and *iNOS* experiments, HIE monolayers were Mock or RV (Ito)-infected and then treated with DMSO, 100U/mL apyrase, or 10 μM BPTU and normalized to 18s mRNA transcripts and relative to the Mock-DMSO condition.

Measurement of serotonin release. Serotonin secretion by HIEs following stimulation with RV infection and treatment with DMSO, 100U/mL apyrase, 10 μM BPTU, or 300 nM ω-agatoxin was quantified by ELISA (Eagle Biosciences) according to the manufacturer's instructions. A standard curve of known serotonin concentrations was plotted against optical density at 450 nm with a limit of detection of 2.6 ng/mL (Infinite F200Pro, Tecan). Experiments in flat monolayers were performed three times independently and experiments in transwells were performed three times independently and data shown are representative of all replicates combined.

Statistical analysis. Biostatistical analyses were performed using GraphPad Prism (version 8.1) software (GraphPad Inc., La Jolla, CA). Outlier data points were removed using the ROUT method (Q = 1%). Statistical comparisons were made using Mann- Whitney test, one-way Analysis of Variance (ANOVA), or the Kruskal-Wallis test and the Tukey, Bonferroni, or Dunn's multiple comparisons test. Differences between the groups were considered significant at $p < 0.05$ (*), and the data are presented as mean ± standard deviation unless otherwise noted. All authors had access to the study data, reviewed, and approved the final manuscript.

Data availability. The data that support the findings of this study are available from the corresponding author upon reasonable request.

References (needs to be ~ 50 references)

1. Troeger, C. *et al.* Rotavirus Vaccination and the Global Burden of Rotavirus Diarrhea among Children Younger Than 5 Years. *JAMA Pediatr.* **172**, 958–965 (2018).

2. Davidson, G. P. *et al.* Immunofluorescence in duodenal mucosa of children with acute enteritis due to a new virus. *J. Clin. Pathol.* **28**, 263–266 (1975).

3. Little, Lynn M.Shadduck, J. A. Pathogenesis of rotavirus infection. *Infect. Immun.* **38**, 755–763 (1982).

4. Morris, A. P. & Estes, M. K. VIII. Pathological consequences of rotavirus infection and its enterotoxin. *Am. J. Physiol. Liver Physiol.* **281**, G303–G310 (2001).

5. Lundgren, O. *et al.* Role of the enteric nervous system in the fluid and electrolyte secretion of rotavirus diarrhea. *Science* **287**, 491–495 (2000).

6. Hyser, J. M., Collinson-Pautz, M. R., Utama, B. & Estes, M. K. Rotavirus disrupts calcium homeostasis by NSP4 viroporin activity. *MBio* **1**, 1–12 (2010).

7. Ball, J. M., Tian, P., Zeng, C. Q., Morris, a P. & Estes, M. K. Age-dependent diarrhea induced by a rotaviral nonstructural glycoprotein. *Science* **272**, 101–104 (1996).

8. Tian, P. *et al.* The rotavirus nonstructural glycoprotein NSP4 mobilizes Ca2+ from the endoplasmic reticulum. *J. Virol.* **69**, 5763–5772 (1995).

9. Kunzelmann, K. *et al.* Expression and function of epithelial anoctamins. *Exp. Physiol.* **285**, 184–192 (2011).

10. Crawford, S. E., Hyser, J. M., Utama, B. & Estes, M. K. Autophagy hijacked through viroporin-activated calcium/calmodulin-dependent kinase kinase-β signaling is required for rotavirus replication. *Proc. Natl. Acad. Sci. U. S. A.* **109**, E3405-13 (2012).

11. Zambrano, J. L. *et al.* Rotavirus Infection of Cells in Culture Induces Activation of RhoA and Changes in the Actin and Tubulin Cytoskeleton. *PLoS One* **7**, e47612 (2012).

12. Beau, I., Cotte-Laffitte, J., Amsellem, R. & Servin, A. L. A protein kinase A-dependent mechanism by which rotavirus affects the distribution and mRNA level of the functional tight junction-associated protein, occludin, in human differentiated intestinal Caco-2 cells. *J. Virol.* **81**, 8579–8586 (2007).

13. Hagbom, M., Sharma, S., Lundgren, O. & Svensson, L. Towards a human rotavirus disease model. *Curr. Opin. Virol.* **2**, 408–418 (2012).

14. Hodges, K. & Gill, R. Infectious diarrhea: Cellular and molecular mechanisms. *Gut Microbes* **1**, 4–21 (2010).

15. Sowmyanarayanan, T. V. *et al.* Nitric oxide production in acute gastroenteritis in Indian children. *Trans. R. Soc. Trop. Med. Hyg.* **103**, 849–51 (2009).

16. Yamashiro, Y., Shimizu, T., Oguchi, S. & Sato, M. Prostaglandins in the plasma and stool of children with rotavirus gastroenteritis. *J. Pediatr. Gastroenterol. Nutr.* **9**, 322–7 (1989).

17. Rodriguez-Diaz, J. *et al.* Role of Nitric Oxide During Rotavirus Infection. *J. Med. Virol.* **78**, 979–985 (2006).

18. Morris, A. P. *et al.* NSP4 elicits age-dependent diarrhea and Ca2+-mediated I- influx into intestinal crypts of CF mice. *Am. J. Physiol. Gastrointest. Liver Physiol.* **277**, 431–444 (1999).

19. Ousingsawat, J. *et al.* Rotavirus toxin NSP4 induces diarrhea by activation of TMEM16A

and inhibition of Na+ absorption. *Pflugers Arch. Eur. J. Physiol.* **461**, 579–589 (2011).

20. Fujii, S. *et al.* PGE 2 is a direct and robust mediator of anion/fluid secretion by human intestinal epithelial cells. *Sci. Rep.* **6**, 1–15 (2016).

21. Mourad, F. H., Turvill, J. L. & Farthing, M. J. G. Role of nitric oxide in intestinal water and electrolyte transport. *Gut* **44**, 143–147 (1999).

22. Hagbom, M. *et al.* Rotavirus stimulates release of serotonin (5-HT) from human enterochromaffin cells and activates brain structures involved in nausea and vomiting. *PLoS Pathog.* **7**, 1–10 (2011).

23. Michelangeli, F., Ruiz, M. C., del Castillo, J. R., Ludert, J. E. & Liprandi, F. Effect of rotavirus infection on intracellular calcium homeostasis in cultured cells. *Virology* **181**, 520–527 (1991).

24. Hyser, J. M. & Estes, M. K. Pathophysiological Consequences of Calcium-Conducting Viroporins. *Annu. Rev. Virol.* **2**, 16.1-16.24 (2015).

25. Crawford, S. E. *et al.* Rotavirus infection. *Nat. Rev. Dis. Prim.* **3**, (2017).

26. Chang-Graham, A. L. *et al.* Rotavirus Calcium Dysregulation Manifests as Dynamic Calcium Signaling in the Cytoplasm and Endoplasmic Reticulum. *Sci. Rep.* **9**, (2019).

27. Sanderson, M. J., Charles, A. C. & Dirksen, E. R. Mechanical stimulation and intercellular communication increases intracellular Ca2+ in epithelial cells. *Cell Regul.* **1**, 585–96 (1990).

28. Cornell-Bell, A. H., Finkbeiner, S. M., Cooper, M. S. & Smith, S. J. Glutamate induces calcium waves in cultured astrocytes: long-range glial signaling. *Science* **247**, 470–3 (1990).

29. Leybaert, L. & Sanderson, M. J. Intercellular Ca(2+) waves: mechanisms and function. *Physiol. Rev.* **92**, 1359–1392 (2012).

30. Seo, N. *et al.* Integrins are receptors for the rotavirus enterotoxin. *Proc. Natl. Acad. Sci.* **105**, 8811–8818 (2008).

31. Emslie, K. R. *et al.* Expression of the rotavirus SA11 protein VP7 in the simple eukaryote Dictyostelium discoideum. *J. Virol.* **69**, 1747–1754 (1995).

32. Sato, T. *et al.* Long-term expansion of epithelial organoids from human colon, adenoma, adenocarcinoma, and Barrett's epithelium. *Gastroenterology* **141**, 1762–1772 (2011).

33. Saxena, K. *et al.* Human Intestinal Enteroids: a New Model To Study Human Rotavirus Infection, Host Restriction, and Pathophysiology. *J. Virol.* **90**, 43–56 (2016).

34. Foulke-Abel, J. *et al.* Human enteroids as an ex-vivo model of host-pathogen interactions in the gastrointestinal tract. *Exp. Biol. Med.* **239**, 1124–1134 (2014).

35. Zachos, N. C. *et al.* Human enteroids/colonoids and intestinal organoids functionally recapitulate normal intestinal physiology and pathophysiology. *J. Biol. Chem.* **291**, 3759–3766 (2016).

36. Léon, C. *et al.* The P2Y1 receptor is an ADP receptor antagonized by ATP and expressed in platelets and megakaryoblastic cells. *FEBS Lett.* **403**, 26–30 (1997).

37. Dickman, K. G. *et al.* Rotavirus alters paracellular permeability and energy metabolism in Caco-2 cells. *Am. J. Physiol. Gastrointest. Liver Physiol.* **279**, G757–G766 (2000).

38. Zhang, C. *et al.* Virus-Triggered ATP Release Limits Viral Replication through Facilitating

IFN-β Production in a P2X7-Dependent Manner. *J. Immunol.* **199**, 1372–1381 (2017).

39. Ferrari, D., Idzko, M., Müller, T., Manservigi, R. & Marconi, P. Purinergic Signaling: A New Pharmacological Target Against Viruses? *Trends Pharmacol. Sci.* **39**, 926–936 (2018).

40. Zumerle, S. *et al.* Intercellular Calcium Signaling Induced by ATP Potentiates Macrophage Phagocytosis. *Cell Rep.* **27**, 1-10.e4 (2019).

41. Cekic, C. & Linden, J. Purinergic regulation of the immune system. *Nat. Rev. Immunol.* **16**, 177–192 (2016).

42. Hernández, P. P. *et al.* Interferon-γ and interleukin 22 act synergistically for the induction of interferon-stimulated genes and control of rotavirus infection. *Nat. Immunol.* **16**, 698–707 (2015).

43. Di Paolo, N. C. & Shayakhmetov, D. M. Interleukin 1α and the inflammatory process. *Nat. Immunol.* **17**, 906–913 (2016).

44. Groß, O. *et al.* Inflammasome Activators Induce Interleukin-1α Secretion via Distinct Pathways with Differential Requirement for the Protease Function of Caspase-1. *Immunity* **36**, 388–400 (2012).

45. Ohtani, Y., Minami, M. & Satoh, M. Expression of inducible nitric oxide synthase mRNA and production of nitric oxide are induced by adenosine triphosphate in cultured rat microglia. *Neurosci. Lett.* **293**, 72–74 (2000).

46. Degagné, E. *et al.* P2Y 2 Receptor Transcription Is Increased by NF-κB and Stimulates Cyclooxygenase-2 Expression and PGE 2 Released by Intestinal Epithelial Cells . *J. Immunol.* **183**, 4521–4529 (2009).

47. Bialowas, S. *et al.* Rotavirus and Serotonin Cross-Talk in Diarrhoea. *PLoS One* **11**, e0159660 (2016).

48. Dekkers, J. F. *et al.* A functional CFTR assay using primary cystic fibrosis intestinal organoids. *Nat. Med.* **19**, 939–945 (2013).

49. Cho, M. S. *et al.* Role of ADP receptors on platelets in the growth of ovarian cancer. *Blood* **130**, 1235–1242 (2017).

50. Verkhratsky, A. & Burnstock, G. Biology of purinergic signalling: Its ancient evolutionary roots, its omnipresence and its multiple functional significance. *BioEssays* **36**, 697–705 (2014).

51. Puhar, A., Tronchère, H., Payrastre, B., Tran Van Nhieu, G. & Sansonetti, P. J. A Shigella Effector Dampens Inflammation by Regulating Epithelial Release of Danger Signal ATP through Production of the Lipid Mediator PtdIns5P. *Immunity* **39**, 1121–1131 (2013).

52. Green, V. A. & Pelkmans, L. A Systems Survey of Progressive Host-Cell Reorganization during Rotavirus Infection. *Cell Host Microbe* **20**, 107–120 (2016).

53. Bhowmick, R. *et al.* Rotaviral enterotoxin nonstructural protein 4 targets mitochondria for activation of apoptosis during infection. *J. Biol. Chem.* **287**, 35004–35020 (2012).

54. Séror, C. *et al.* Extracellular ATP acts on P2Y2 purinergic receptors to facilitate HIV-1 infection. *J. Exp. Med.* **208**, 1823–1834 (2011).

55. Berkova, Z., Crawford, S. E., Blutt, S. E., Morris, A. P. & Estes, M. K. Expression of Rotavirus NSP4 Alters the Actin Network Organization through the Actin Remodeling Protein Cofilin. *J. Virol.* **81**, 3545–3553 (2007).

56. Takada, H., Furuya, K. & Sokabe, M. Mechanosensitive ATP release from hemichannels and Ca 2 + influx through TRPC6 accelerate wound closure in keratinocytes. *J. Cell Sci.* **127**, 4159–4171 (2014).

57. Sung, Y. *et al.* Intercellular calcium waves mediate preferential cell growth toward the wound edge in polarized hepatic cells. *Exp. Cell Res.* **287**, 209–218 (2003).

58. Novak, I. Purinergic signalling in epithelial ion transport: regulation of secretion and absorption. *Acta Physiol.* **202**, 501–522 (2011).

59. Perry, J. L., Ramachandran, N. K., Utama, B. & Hyser, J. M. Use of genetically-encoded calcium indicators for live cell calcium imaging and localization in virus-infected cells. *Methods* (2015). doi:10.1016/j.ymeth.2015.09.004

60. Chang-Graham, A. L. *et al.* Human intestinal enteroids with inducible neurogenin-3 expression as a novel model of gut hormone secretion. *Cell. Mol. Gastroenterol. Hepatol.* **0**, (2019).

61. VanDussen, K. L. *et al.* Development of an enhanced human gastrointestinal epithelial culture system to facilitate patient-based assays. *Gut* **64**, 911–920 (2015).

62. Ettayebi, K. *et al.* Replication of human noroviruses in stem cell – derived human enteroids. **5211**, (2016).

63. Estes, M. K., Graham, D. Y., Gerba, C. P. & Smith, E. M. Simian rotavirus SA11 replication in cell cultures. *J. Virol.* **31**, 810–5 (1979).

64. Matrosovich, M., Matrosovich, T., Garten, W. & Klenk, H.-D. New low-viscosity overlay medium for viral plaque assays. *Virol. J.* **3**, 63 (2006).

65. Maynard, J. P. *et al.* P2X3 purinergic receptor overexpression is associated with poor recurrence-free survival in hepatocellular carcinoma patients. *Oncotarget* **6**, (2015).

66. Ren, H. *et al.* Toll-Like Receptor-Triggered Calcium Mobilization Protects Mice against Bacterial Infection through Extracellular ATP Release. *Infect. Immun.* **82**, 5076–5085 (2014).

Supplementary Information is linked to the online version of the paper at www.nature.com/nature.

Acknowledgements

This work was supported in part by NIH grants K01DK093657, R03DK110270, R01DK115507 (PI: J. M. Hyser), and R01AI080656 and U19AI116497 (PI: M. K. Estes). Trainee support for A.C.G. was provided by NIH grants F30DK112563 (PI: A. Chang-Graham) and the BCM Medical Scientist Training Program and support for both A.C.G. and A.C.S. was provided by the Integrative Molecular and Biomedical Sciences Graduate Program (T32GM008231, PI: D. Nelson). This project was supported in part by PHS grant P30DK056338, which supports the Texas Medical Center Digestive Diseases Center (TMC-DDC) Gastrointestinal Experimental Model Systems (GEMS) Core and the Cellular and Molecular Morphology Core. We would like to thank Xi-Lei (Shelly) Zeng and Xiaomin Yu for their help with enteroid cultures and media. FACS sorting of cell lines utilized the BCM Cytometry and Cell Sorting Core with funding from the CPRIT Core Facility Support Award (CPRIT-RP180672), the NIH (CA125123 and RR024574), and the expert assistance of Joel M. Sederstrom. Additional thanks to the BCM Center for Comparative Medicine and technicians for their care of the animals.

Author Contributions

JH, ACG, JLP, MAE, HD, and MKE designed the experiments and discussed the data. JH, ACG, JLP, FS, AS, JN, and JK conducted the calcium imaging experiments and analyzed the data with JH and ACG. JLP conducted the fluorescent focus assays, plaque assays, and genotyping and analyzed data with JH. JLP and ACG created the CRISPR/Cas9 knockout lines. MAE and KE conducted and analyzed qPCR experiments with ACG. HD performed and analyzed the serotonin ELISAs. ACG conducted and analyzed the enteroid swelling assays. JH and ACG performed the mouse experiments and MAE performed immunohistochemistry. NP and MKE provided key

reagents including the anti-NSP4 antibodies. SK provided the P2Y1-null mice. JH and ACG wrote the manuscript, and all authors contributed to revisions of the paper.

Author Information

Reprints and permissions information is available at www.nature.com/reprints. The authors declare no competing financial interests. Correspondence and requests for materials should be addressed to Joseph Hyser, Joseph.Hyser@bcm.edu

Figures (legends must be < 100 words, total 500 words for paper, put more info into methods)

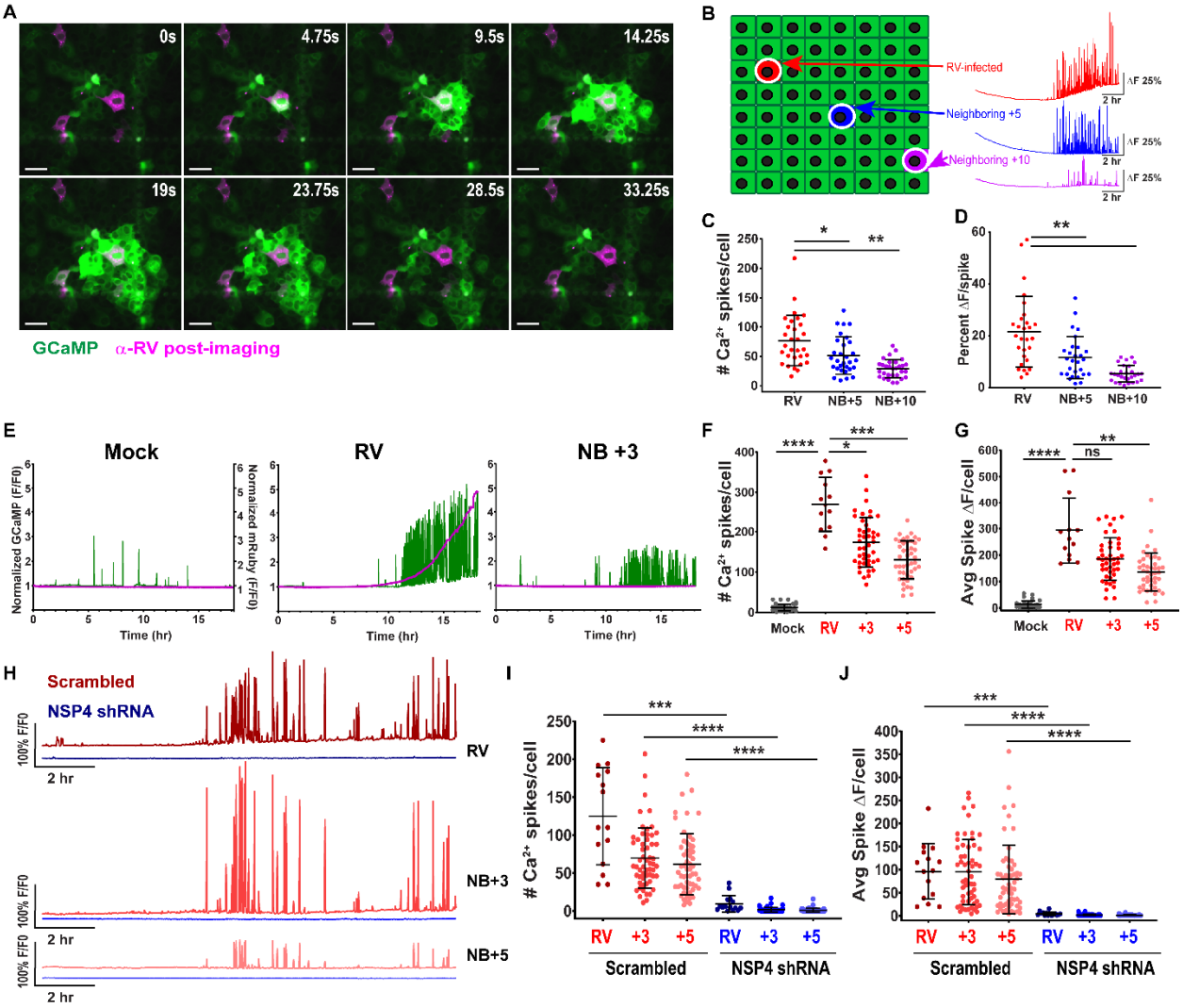

Figure 1. Rotavirus-infected cells trigger calcium signaling in neighboring uninfected cells. (A) MA104-GCaMP cells, RV (SA114F)-infected (pink). Scale bar = 100 µm. **(B)** Representative Ca^{2+} traces of normalized GFP fluorescence (F/F_0) of RV-infected cell and neighboring (NB) cells. **(C, F, I)** Ca^{2+} spikes per cell and **(D, G, J)** average F/F_0 increase of Ca^{2+} spike/cell **(E-G)** Mock- or RV (SA11cl3-mRuby3)-infected, **(E)** representative Ca^{2+} traces Left axis: GCaMP F/F_0 (green), Right axis: mRuby3 F/F_0 (pink)**. (H-J)** MA104-GCaMP-shRNA scrambled or shRNA-NSP4 cells infected with RV (SA11cl3-mRuby3), **(H)** Representative Ca^{2+} traces. Kruskal-Wallis with Dunn's multiple comparisons test. (*p<0.05, **p<0.01, ***p<0.001, ****p<0.0001)

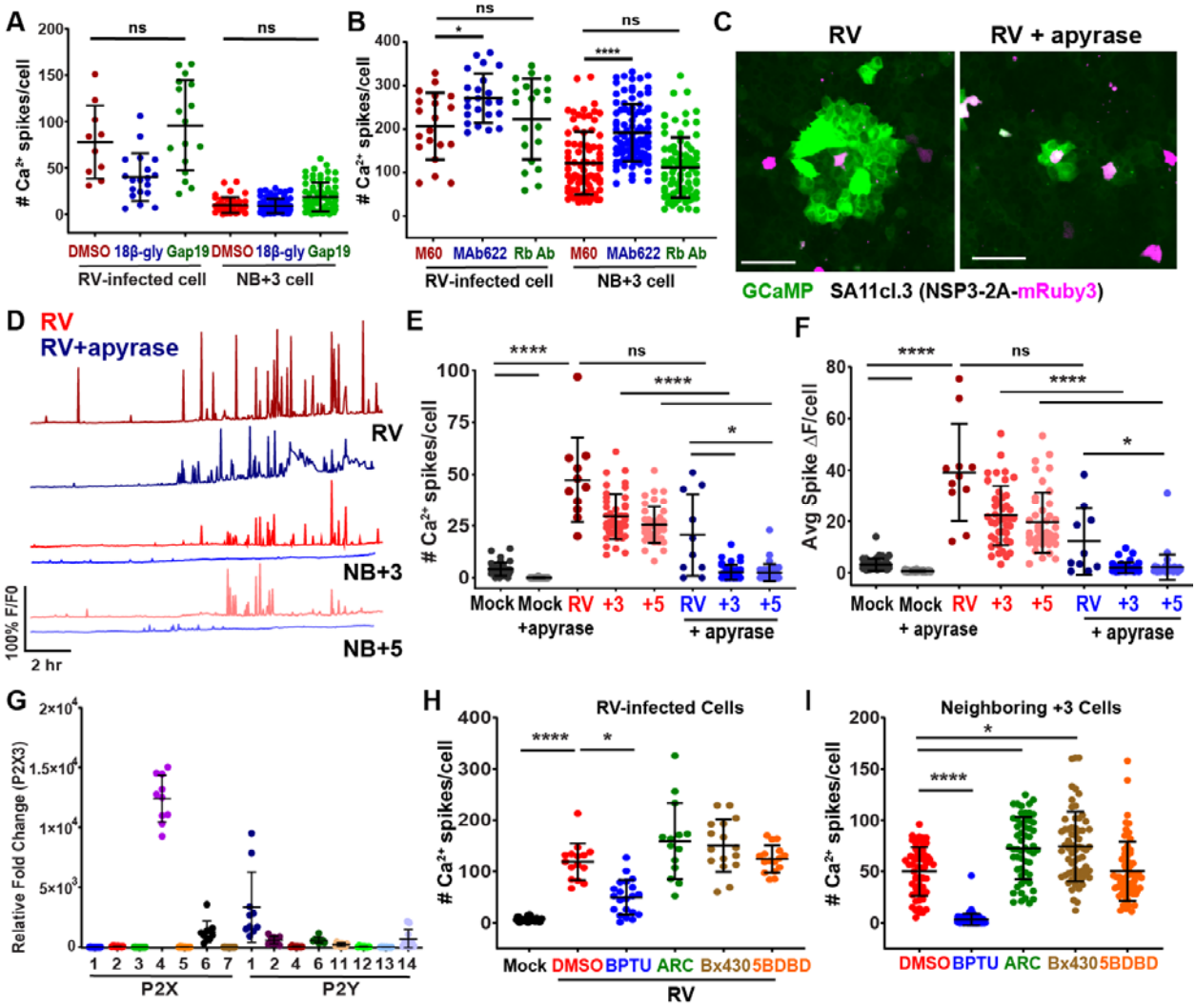

Figure 2. Rotavirus induces intercellular calcium waves by activating purinergic signaling. **(A-B)** Ca^{2+} spikes in MA104-GCaMP cells in RV-infected (SA11cl3-mRuby3) and neighboring (NB)+3 cell, treated with: **(A)** DMSO or gap junction blockers or **(B)** anti-VP7 M60 MAb, anti-NSP4 MAb 622, or anti-NSP4 antisera 120-147 (Rb Ab). **(C)** RV-infected cells, mock- or apyrase-treated and **(D)** representative Ca^{2+} traces. **(E)** Ca^{2+} spikes and **(F)** average F/F_0 increase of Ca^{2+} spikes. **(G)** qPCR of purinergic receptor mRNA transcripts in MA104 cells. **(H-I)** Ca^{2+} spikes in RV-infected **(H)** or NB **(I)** cells treated with DMSO or purinergic receptor blockers. Kruskal-Wallis with Dunn's multiple comparisons test. (Scale bar = 100 μm) (*p<0.05, ****p<0.0001)

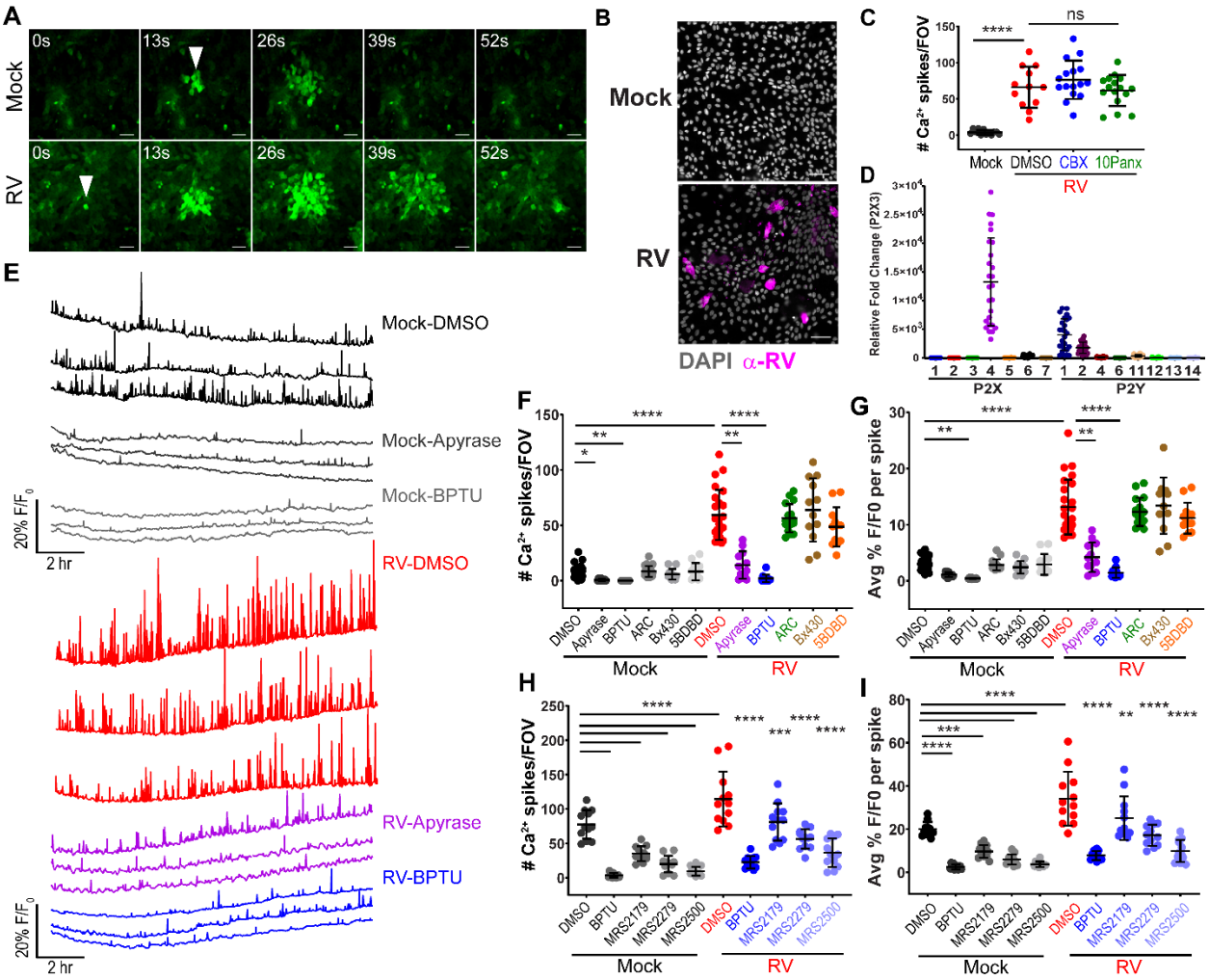

Figure 3. Rotavirus infection induces intercellular waves in human intestinal enteroids. **(A)** Patient J3 jHIE-GCaMP6s monolayers mock- or RV(Ito)-infected (ICW, arrowhead) and **(B)** immunofluorescence. **(C)** Ca^{2+} spikes per field-of-view (FOV), in (J3)HIEs mock- or RV-infected and treated with vehicle, 100 μM carbenoxolone, or 10 μM 10Panx. **(D)** qPCR of purinergic receptor mRNA transcripts in (J3)HIEs. **(E-G)** Mock- or RV-infected (J3)HIEs, treated with DMSO, apyrase, or purinergic receptor blockers, **(E)** Ca^{2+} traces, **(F)** Ca^{2+} spikes/FOV, and **(G)** average F/F_0 increase of Ca^{2+} spikes. **(H)** Ca^{2+} spikes/FOV of patient J2 jHIE-GCaMP6s monolayers mock- or RV-infected and treated with DMSO or P2Y1 receptor blockers, and **(I)** average F/F_0 increase of Ca^{2+} spikes. One-way ANOVA with Bonferroni's **(C,H,I)** and Kruskal-Wallis with Dunn's **(F,G)** multiple corrections test. (*p<0.05, **p<0.01, ***p<0.001, ****p<0.0001) scale bar = 50 μm.

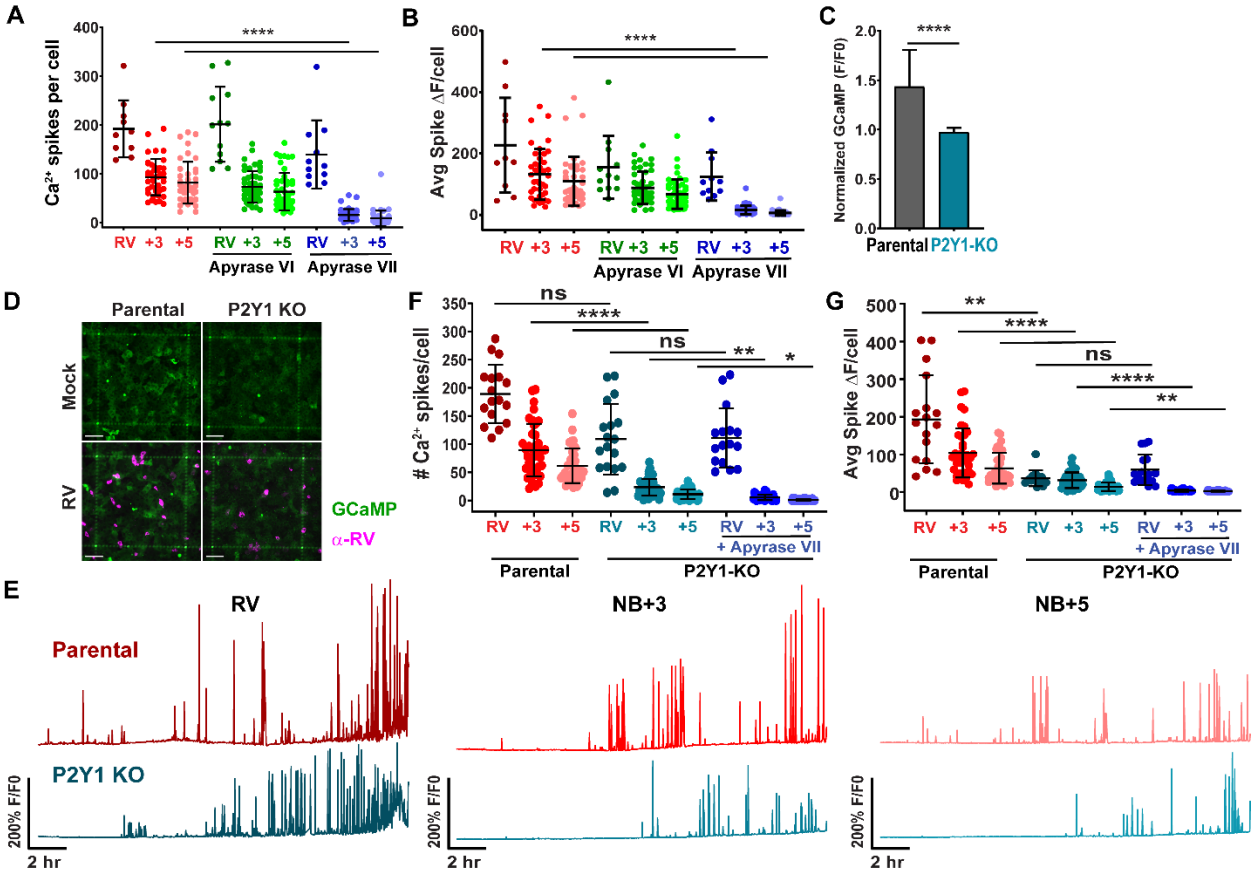

Figure 4. CRISPR/Cas9 knockout of P2Y1 receptor reduces intercellular calcium waves. **(A)** Ca^{2+} spikes and **(B)** average F/F_0 increase of Ca^{2+} spikes in MA104-GCaMP cells infected with RV (SA114F) and treated with apyrase VI or VII. **(C)** F/F_0 increase in parental or P2Y1 KO MA104-GCaMP cells treated with 1 nM ADP. Mann-Whitney test. **(D)** Immunofluorescence of parental or P2Y1ko cells mock- or RV-infected (pink). Scale bar = 100 µm **(E)** Ca^{2+} traces of parental or P2Y1ko cells infected with RV (SA11cl3-mRuby3). **(F)** Ca^{2+} spikes/cell in RV-infected or NB +3 or +5 cell and **(G)** the average F/F_0 increase per spike. **(A-B, F-G)** Kruskal-Wallis with Dunn's multiple comparisons test. (*$p< 0.05$, **$p<0.01$, ****$p<0.0001$)

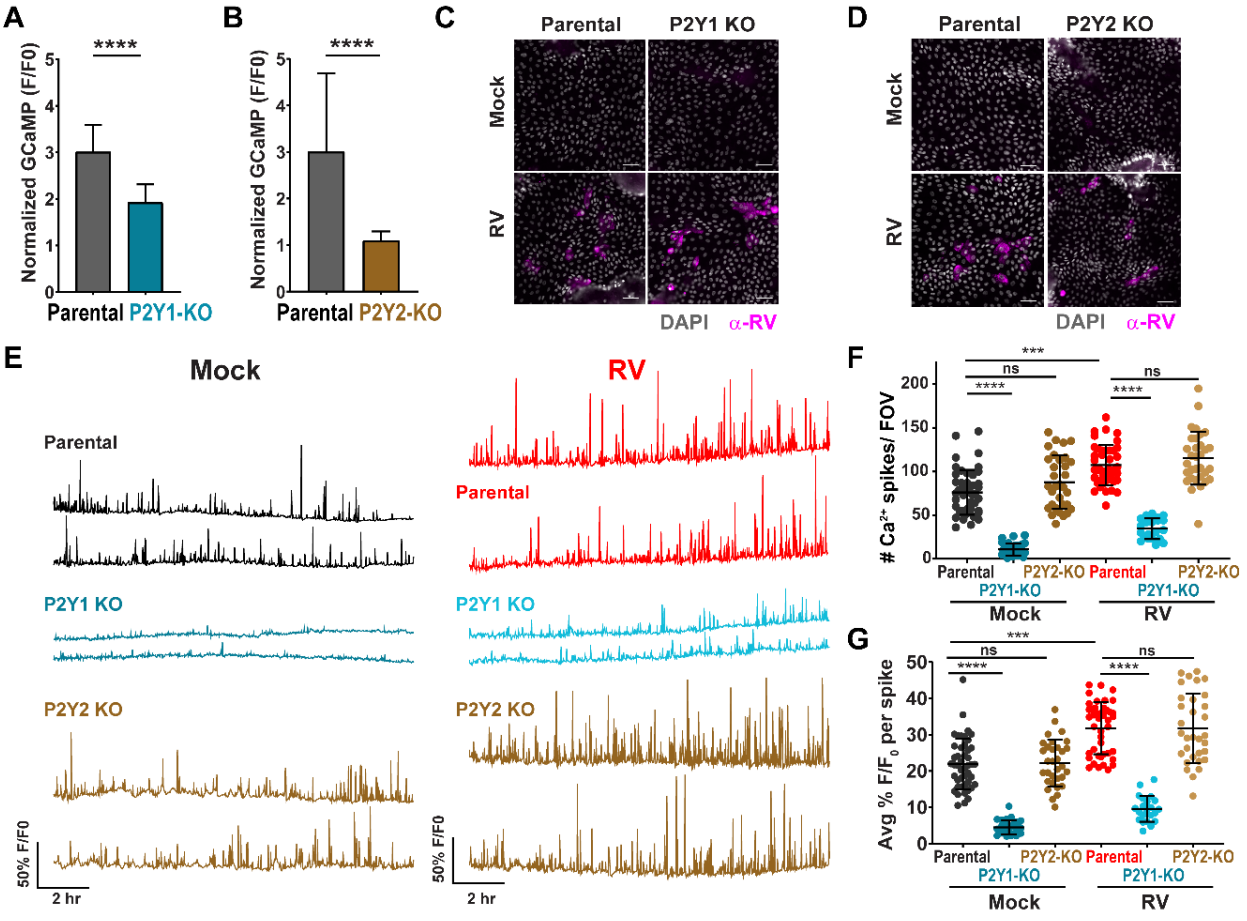

Figure 5. CRISPR/Cas9 knockout of P2Y1 receptor in jHIEs reduces intercellular calcium waves.

(A-B) F/F_0 increase in parental or **(A)** P2Y1ko (J2)HIE-GCaMP6s monolayers treated with 10 nM ADP and **(B)** P2Y2ko (J2)HIE-GCaMP6s monolayers treated with 10 μM ATP-γS. Mann-Whitney test. **(C-D)** Parental, P2Y1ko, or P2Y2ko jHIE-GCaMP6s monolayers mock- or RV(Ito)-infected, immunostained for RV antigen (pink). **(E)** Ca^{2+} traces/FOV of mock- or RV-infected **(F)** Ca^{2+} spikes/FOV and **(G)** average F/F_0 increase. Mann-Whitney **(A-B)** or Kruskal-Wallis test with Dunn's multiple corrections test **(F-G)**. (***p<0.001, ****p<0.0001) Scale bar = 50 μm.

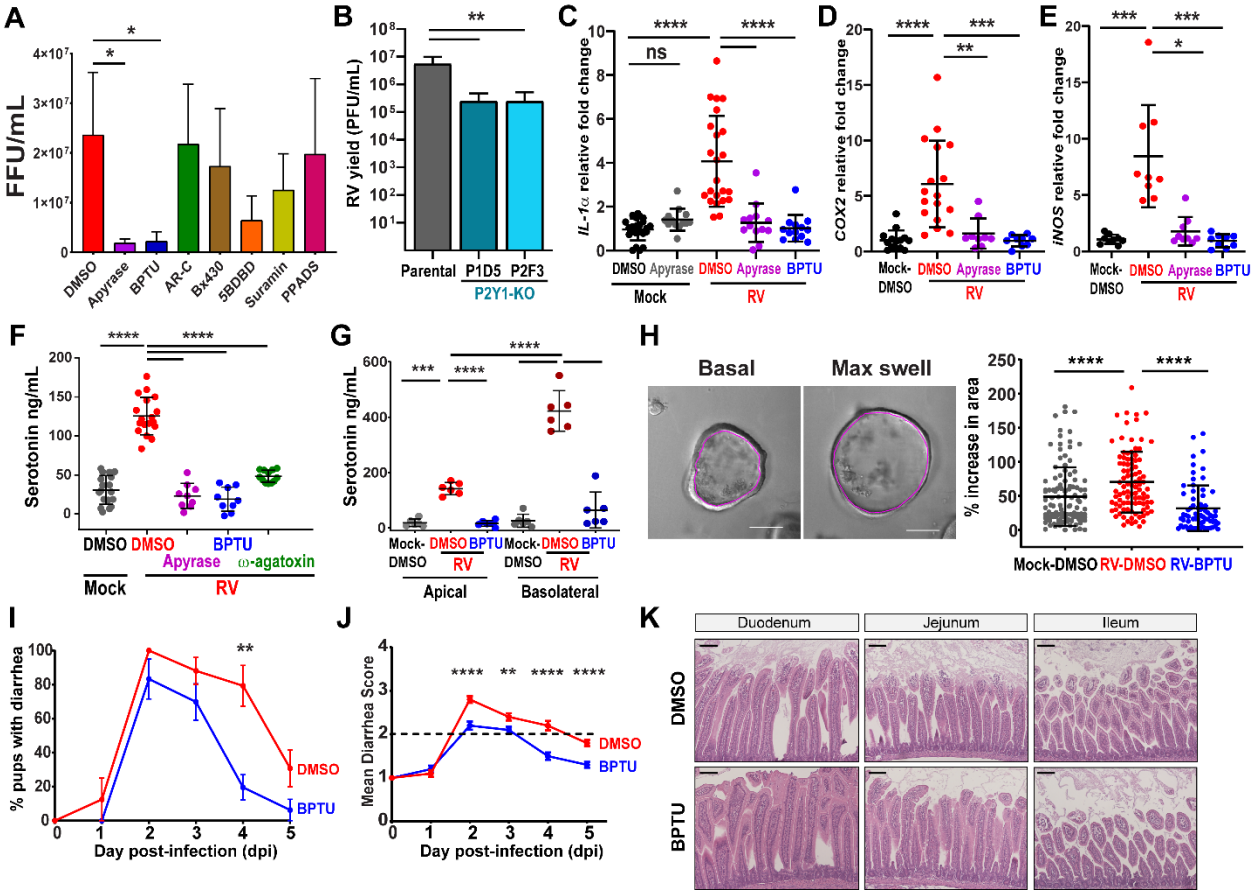

Figure 6. Purinergic signaling contributes to rotavirus disease processes.
(A) Fluorescent focus yield of RV(SA114F)-infected MA104 cells. **(B)** Plaque yield of RV (SA114F)-infected MA104-GCaMP or MA104-GCaMP-P2Y1ko cells. **(C-E)** qPCR of mRNA transcripts in jHIE monolayers **(F-G)** Serotonin secretion from RV-infected jHIE **(F)** monolayers and **(G)** transwells. **(H)** Enteroid swelling assay using mock- or RV(Ito)-infected jHIEs treated with DMSO or 10 μM BPTU. **(I-K)** C57Bl/6J mouse pups with diarrhea infected with Rhesus RV and vehicle- or BPTU-treated and the **(J)** mean diarrhea score. Mean ± SEM. **(K)** Hematoxylin and eosin-stained intestinal sections, 5 dpi. Mann-Whitney **(H-J)**, Kruskal-Wallis with Dunn's multiple comparisons **(C-E)** or one-way ANOVA with Bonferroni multiple comparisons test **(A-B, F-G).** (*p<0.05, **p<0.01, ***p<0.001, ****p<0.0001). Scale bar = 100 μm.

Extended Data Figures

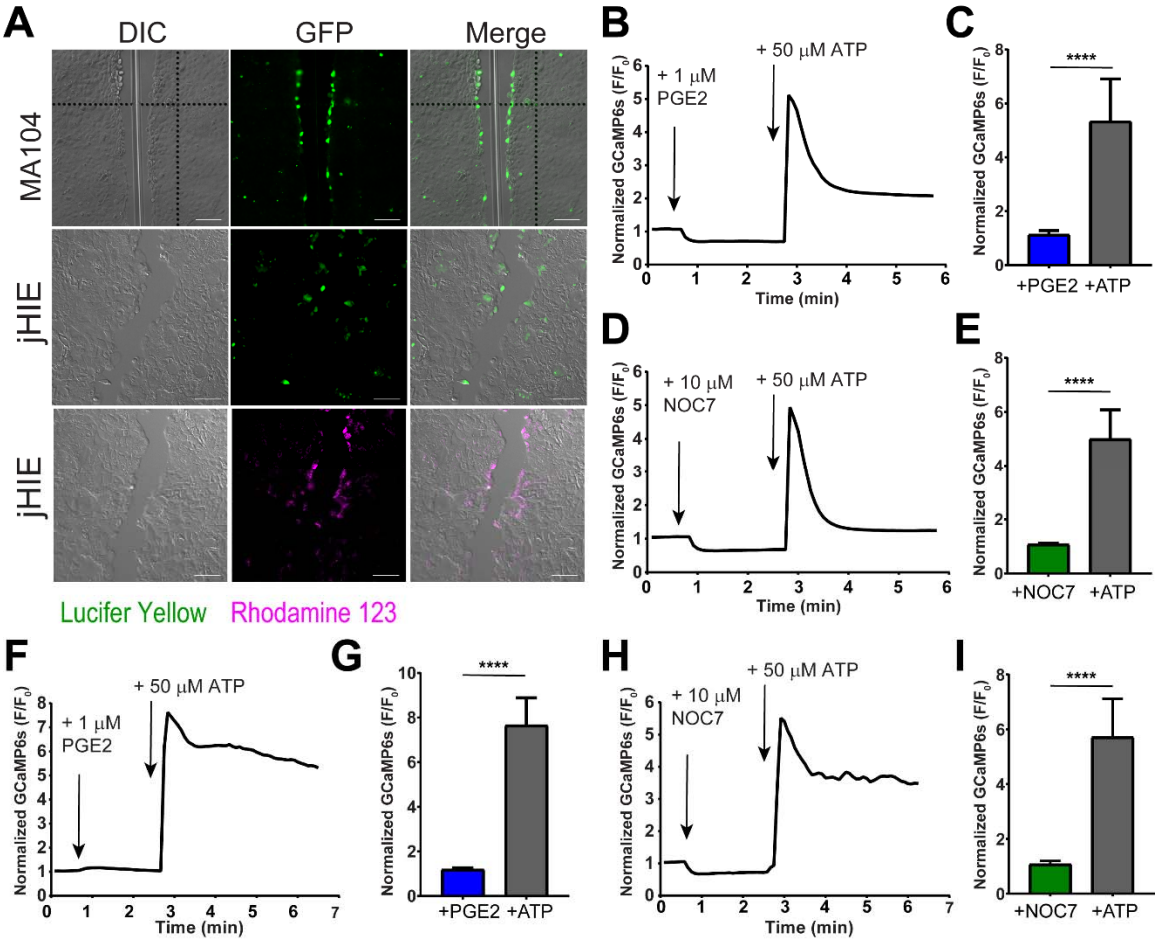

Figure S1. Rotavirus-induced Ca^{2+} waves do not occur *via* gap junctions, prostaglandin E2, or nitric oxide.
(A) Dye loading scratch assay with Lucifer Yellow and Rhodamine 123 in MA104 cells and jHIE (patient J3) monolayers. scale bar = 100 μm. **(B-C)** MA104-GCaMP6s cells treated with 1 μM prostaglandin E2 (PGE2) followed by 50 μM ATP with **(B)** normalized GFP fluorescence average trace and **(C)** maximum normalized GCaMP6s fluorescence increase. **(D-E)** MA104-GCaMP6s cells treated with 10 μM NOC7 followed by 50 μM ATP with **(D)** normalized GFP fluorescence average trace and **(E)** maximum normalized GCaMP6s fluorescence increase. **(F-G)** jHIE-GCaMP6s cells (patient J2) treated with 1 μM PGE2 followed by 50 μM ATP with **(F)** normalized GFP fluorescence average trace and **(G)** maximum normalized GCaMP6s fluorescence increase. **(H-I)** jHIE-GCaMP6s cells (patient J2) treated with 10 μM NOC7 followed by 50 μM ATP with **(H)** normalized GFP fluorescence average trace and **(I)** maximum normalized GCaMP6s fluorescence increase. (For **B-I**), n = 30 cells, Mann-Whitney test. Data representative of 4 replicate experiments (****p<0.0001).

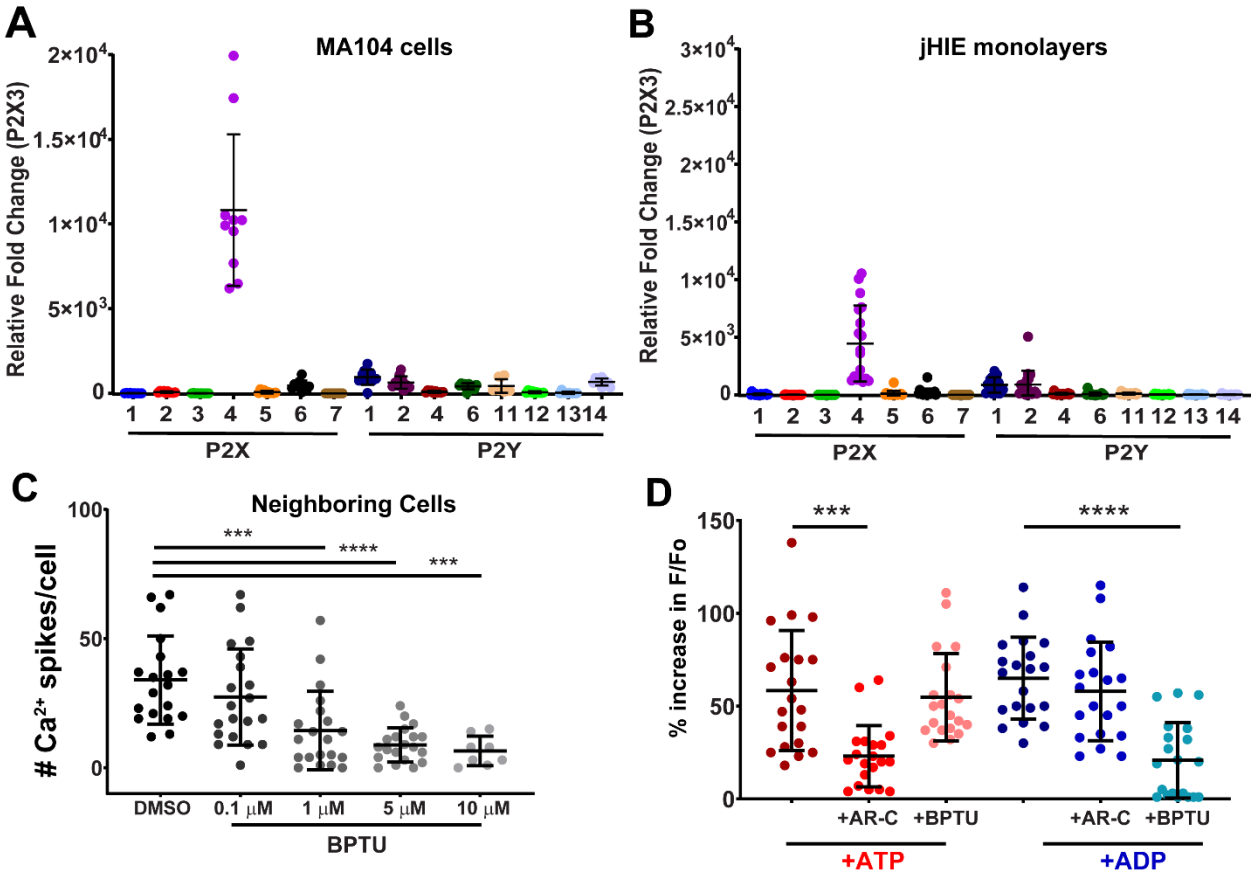

Figure S2. Purinergic blockers of P2Y1 reduce rotavirus-induced calcium waves. **(A-B)** qPCR of purinergic receptor mRNA transcripts relative to P2X3 mRNA transcript levels in **(A)** RV (SA114F)-infected MA104 cells or **(B)** RV (Ito)-infected jHIE monolayers. **(C)** Ca^{2+} spikes in NB cells of RV(SA114F)-infected MA104-GCaMP cells treated with DMSO or BPTU. (n= 20 cells, 3 replicates) **(D)** Normalized relative GFP fluorescence of MA104-GCaMP cells incubated with 10 μM AR-C 118925XX (AR-C) or 10 μM BPTU for 3.5 min before addition with 10 nM ADP or 1 μM ATP (n= 20 cells, 3 replicates each). Kruskal-Wallis with Dunn's comparisons test (***$p<0.001$, ****$p<0.0001$).

Figure S3. Genotyping of P2Y1 Knockout Cells.
(A) Sequencing chromatogram and **(B)** genotyping of P2Y1 receptor knockout in MA104-GCaMP-P2Y1ko cells. Parental P2Y1 receptor sequence compared to 3 alleles, mutations in red. **(C)**

Sequence chromatogram and **(D)** genotyping of P2Y1 receptor knockout in jejunum HIE-GCaMP6s-P2Y1ko cells. Parental P2Y1 receptor sequence compared to 2 alleles of the P2Y1 receptor knockouts with an insertion (black arrow) and deletion (dashed line) indicated. The sequence shown is 648 nucleotides relative to the P2Y1 receptor start codon. Small guide RNA sequences highlighted in yellow.

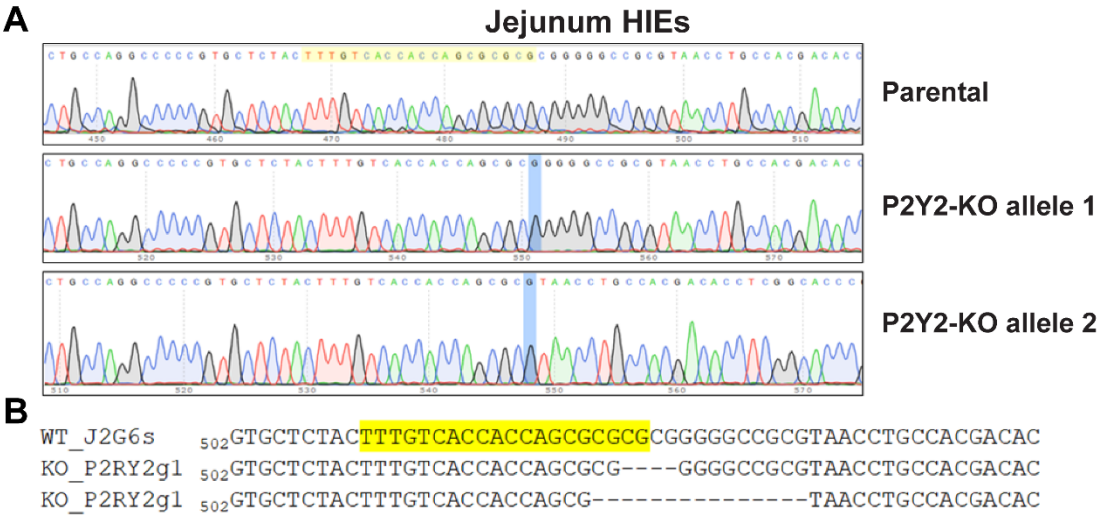

Figure S4. Genotyping of P2Y1 Knockout HIEs.
(A) Sequence chromatogram and **(B)** genotyping of P2Y2 receptor knockout in jejunum HIE-GCaMP6s-P2Y2ko cells. Parental P2Y2 receptor sequence is compared to 2 alleles from the P2Y2 receptor knockouts with the sites of mutation highlighted in blue. Small guide RNA sequence highlighted in yellow. The sequence shown is 502 nucleotides relative to the P2Y2 receptor start codon.

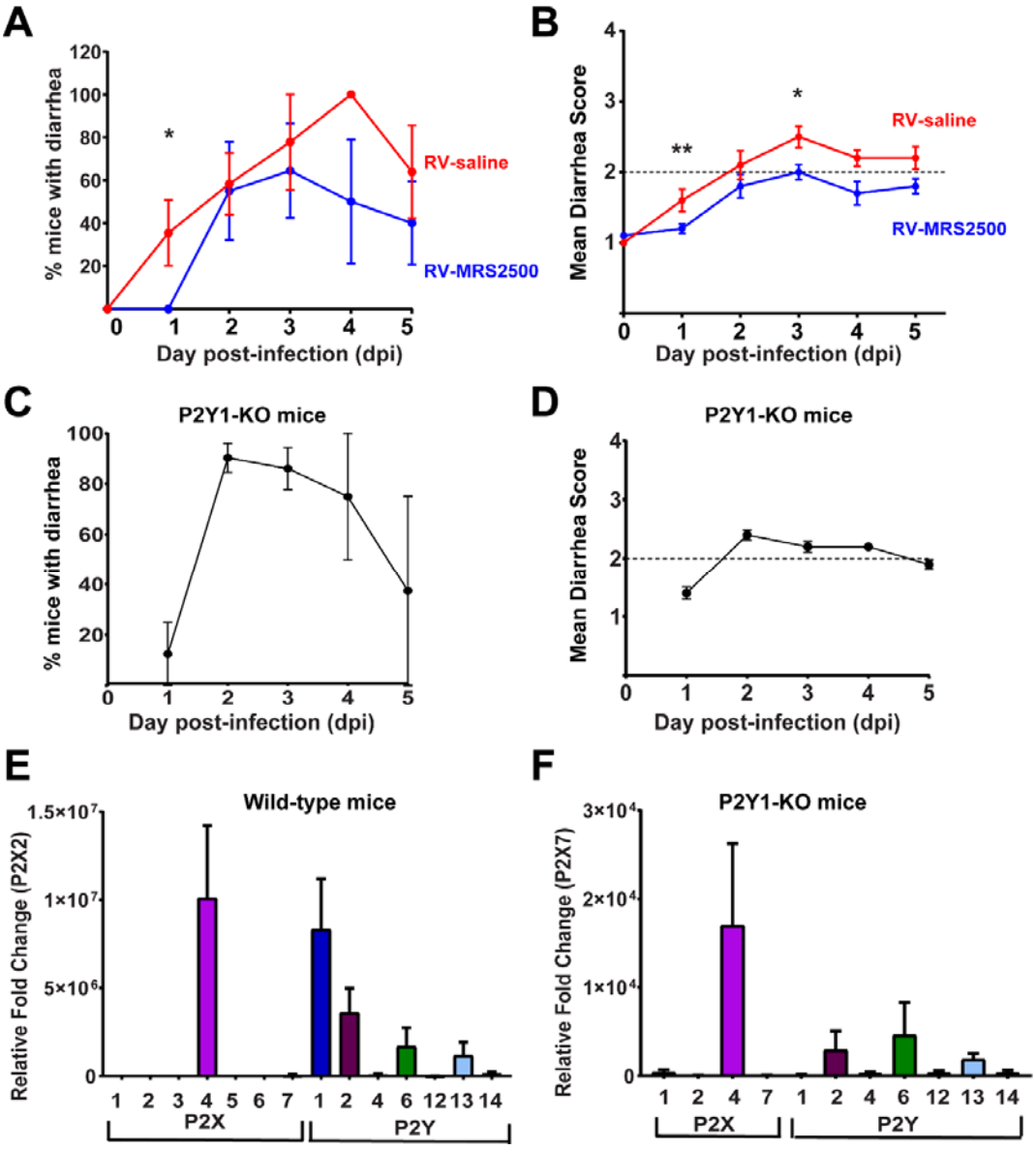

Figure S5. P2Y1 receptor blocker MRS2500 and P2Y1 receptor-null neonatal mice have attenuated rotavirus diarrhea.
(A) Percentage of C57Bl/6J mouse pups with diarrhea infected with Rhesus RV and vehicle- or MRS2500-treated and the **(D)** mean diarrhea score. **(C)** Percentage of P2Y1$^{-/-}$ mouse pups with diarrhea infected with Rhesus RV and the **(D)** mean diarrhea score. **(E)** qPCR of purinergic receptor mRNA transcripts from C57Bl/6J background neonatal mouse jejunum (n = 3 replicates). **(F)** qPCR of purinergic receptor mRNA transcripts from P2Y1-/- neonatal mouse jejunum (n = 2 replicates). **(A-D)** Mann-Whitney test, data presented as mean ± SEM (*p<0.05, **p<0.01).

Extended Data Tables

Extended DataTable 1: Genotyping primers

Gene Target	Species	Product size	Forward (5') Sequence	Reverse (3') Sequence
P2RY1 -WT	Mouse	252 bp	GAAACAGTACTGTCGCCTCAAC	CTCGCTCCTCCTGGAAGCTTTC
P2RY1 -null	Mouse	960 bp	GCAGCGCATCGCCTTCTATC	GGATATGTGCATCAAATTGATG
P2RY1	Human	954 bp	CAGACTGGATCTTCGGGGATGCC	CCCGCCAAGAAATAGAGAATGGGG
P2RY2	Human	1025 bp	CCTGGAATGACACCATCAATGGC	CCTCTGCATGTCAGTTCTGTCG

Extended Table 2: qPCR primer sequences

Gene	Species	Forward (5') Sequence	Reverse (3') Sequence	Citation
18S	Universal	CGCCTTCCTCTTCGAGTATGA	AGATAACGCCCACCTTCTTATTACG	
IL-1α	Human	GAATGACGCCCTCAATCAAAGT	TCATCTTGGGCAGTCACATACA	
COX2	Human	ATCATTCACCAGGCAAATTGC	GGCTTCAGCATAAAGCGTTTG	
iNOS	Human	CAGCTCCACAAGCTGGCTCG	CAGGATGTCCTGAACGTAGACCTTG	
P2X1	Human	CGCCTTCCTCTTCGAGTATGA	AGATAACGCCCACCTTCTTATTACG	65
P2X2	Human	GCCTACGGGATCCGCATT	TGGTGGGAATCAGGCTGAAC	
P2X3	Human	GCTGGACCATCGGGATCA	GAAAACCCACCCTACAAAGTAGGA	
P2X4	Human	CCTCTGCTTGCCCAGGTACTC	CCAGGAGATACGTTGTGCTCAA	
P2X5	Human	CTGCCTGTCGCTGTTCGA	GCAGGCCCACCTTCTTGTT	
P2X6	Human	AGGCCAGTGTGTGGTGTTCA	TCTCCACTGGGCACCAACTC	
P2X7	Human	TCTTCGTGATGACAAACTTTCTCAA	GTCCTGCGGGTGGGATACT	
P2Y1	Human	CGTGCTGGTGTGGCTCATT	GGACCCCGGTACCTGAGTAGA	
P2Y2	Human	GAACTGACATGCAGAGGATAGAAGAT	GCCGGCGTGGACTCTGT	
P2Y4	Human	CCGTCCTGTGCCATGACA	TGACCGCCGAGCTGAAGT	
P2Y6	Human	GCCGGCGACCACATGA	GACCCTGCCTCTGCCATTT	
P2Y11	Human	CTGGAGCGCTTCCTCTTCAC	GGTAGCGGTTGAGGCTGATG	
P2Y12	Human	AGGTCCTCTTCCCACTGCTCTA	CATCGCCAGGCCATTTGT	
P2Y13	Human	GAGACACTCGGATAGTACAGCTGGTA	GCAGGATGCCGGTCAAGA	
P2Y14	Human	TTCCTTTCAAGATCCTTGGTGACT	GCAGAGACCCTGCACACAAA	
P2X1	Mouse	CAGTTCTCTGTGATCTCTTATTG	GTCCTCCGCATACTTGAA	66
P2X2	Mouse	TTCACCATCCTCATCAAG	TCAGGTAGTCACTCTTCT	
P2X3	Mouse	CCCTATTTGTGCTATTAG	TTCTATTCTGTTCTCTTAC	
P2X4	Mouse	TACGAGCAGGGTCTTTCCGGA	ACAAGACGTGCTCGGGCAAC	
P2X5	Mouse	CCACACTATTATTTCAAC	CCATTAACTATCACATCA	
P2X6	Mouse	CTCAAGCTCTATGGAATC	CTTGCCTCTTCATATTTG	
P2X7	Mouse	GAACCCAAGCCGACGTTGAAGT	GACAGCCTAGACAGGTCGGAGA	
P2Y1	Mouse	CGCACACAGGTACAGTGGCGT	TTCCGAGTCCCAGTGCCAGAGT	
P2Y2	Mouse	GTGCGGGGAACCCGGATCAC	AGCCGCCTGGCCATAAGCAC	
P2Y4	Mouse	GTGTGCACCGCTACATGGGCA	TCAGGCAGAGTCGTGTCATGGCA	
P2Y6	Mouse	AGGGGACCACTGGCCCTTCG	TACCCAAGCAGCACGGCGAC	
P2Y11	Mouse	CAGAGTTTGGTCTAGTTTGGCACGA	TGGGAACTTTGGCTGAACCCCT	
P2Y12	Mouse	GGGCCTCATCGCTTTCGACAGG	TCACGGATGATGGCGTTGCCT	
P2Y13	Mouse	GGGGCGGAAGTGGCACAAGG	GCGGCTGGACTTCCTCTTGACG	
P2Y14	Mouse	CAGTTCTCTGTGATCTCTTATTG	GTCCTCCGCATACTTGAA	

For **Supplementary Video and Audio file**s, please provide a one-sentence title and a short legend (no more than 100 words and without reference citations) for each video/audio file. Please include this information in a separate editable file (or include in the SIGuide document) and not in the main SI PDF. Ensure that **discrete pieces of the SI (for example, videos) are referred to at least once** in the print version of the paper at an appropriate point in the text

Supplementary Video 1. Rotavirus infection induces calcium signaling beyond the infected cell.

MA104-GCaMP cells were infected with rotavirus (strain SA114F) and live time-lapse imaging was performed at approximately 18 hr post infection. Images were captured at 1 second intervals for 3 minutes. GCaMP reports cytoplasmic Ca^{2+} as changes in fluorescence intensity (green) and images of RV-antigen positive cells by immunofluorescence (pink) were superimposed on the movies. Note the imbedded timer displays time from the beginning of acquisition not the time post-infection.

Supplementary Video 2. Rotavirus-infected cells elicit intercellular calcium waves.

MA104-GCaMP5G cells were mock-inoculated or rotavirus-infected with the recombinant SA11cl3-mRuby3 reporter virus and live time-lapse imaging was performed. GCaMP5G reports cytoplasmic Ca^{2+} as changes in fluorescence intensity (green) and rotavirus protein synthesis is reported by mRuby3 expression (pink) from the nonstructural protein 3 (NSP3) open-reading frame. Note the imbedded timer displays time from the beginning of acquisition not the time post-infection.

Supplementary Video 3. Blocking enterotoxin NSP4 signaling does not reduce intercellular calcium waves in rotavirus infection.

MA104-GCaMP cells were rotavirus-infected with the recombinant SA11cl3-mRuby3 reporter virus and live time-lapse imaging was performed. GCaMP5G reports cytoplasmic Ca^{2+} as changes in fluorescence intensity (green) and rotavirus protein synthesis is reported by mRuby3 expression (pink) from the nonstructural protein 3 (NSP3) open-reading frame. Cells were left untreated or treated with anti-VP7 M60 MAb, anti-NSP4 MAb 622, or purified antibody for anti-NSP4 120-147 antisera (Rb Ab) after infection. Note the imbedded timer displays time from the beginning of acquisition not the time post-infection.

Supplementary Video 4. Blocking purinergic signaling inhibits intercellular calcium waves in rotavirus infection.

MA104-GCaMP cells were mock-inoculated or rotavirus-infected with the recombinant SA11cl3-mRuby3 reporter virus and live time-lapse imaging was performed. GCaMP5G reports cytoplasmic Ca^{2+} as changes in fluorescence intensity (green) and rotavirus protein synthesis is reported by mRuby3 expression (pink) from the nonstructural protein 3 (NSP3) open-reading frame. Cells were treated with 10 U/mL apyrase after infection. Note the imbedded timer displays time from the beginning of acquisition not the time post-infection.

Supplementary Video 5. Blocking the P2Y1 receptor inhibits intercellular calcium waves in rotavirus infection.

MA104-GCaMP cells were mock-inoculated or rotavirus-infected with the recombinant SA11cl3-mRuby3 reporter virus and live time-lapse imaging was performed. GCaMP5G reports cytoplasmic Ca^{2+} as changes in fluorescence intensity (green) and rotavirus protein synthesis is reported by mRuby3 expression (pink) from the nonstructural protein 3 (NSP3) open-reading frame. Cells were treated with 10 μM BPTU after infection. Note the imbedded timer displays time from the beginning of acquisition not the time post-infection.

Supplementary Video 6. Rotavirus infection induces intercellular calcium waves in human intestinal enteroids.
Jejunum HIE-GCaMP6s enteroid monolayers were mock- or rotavirus (strain Ito)-infected, and imaged once per minute for ~7-22 hpi. GCaMP6s reports cytoplasmic Ca^{2+} as changes in fluorescence intensity (green). Note the imbedded timer displays time from the beginning of acquisition not the time post-infection.

Supplementary Video 7. Blocking purinergic signaling and P2Y1 receptor inhibits intercellular calcium waves in human intestinal enteroids.
Jejunum HIE-GCaMP6s enteroid monolayers were mock- or rotavirus (strain Ito)-infected, and treated with vehicle (DMSO), 100 U/mL apyrase, or 10 μM BPTU and imaged once per minute for ~7-22 hpi. GCaMP6s reports cytoplasmic Ca^{2+} as changes in fluorescence intensity (green). Note the imbedded timer displays time from the beginning of acquisition not the time post-infection.

Supplementary Video 8. CRISPR/Cas9 knockout of the P2Y1 receptor reduces intercellular calcium waves.
MA104-GCaMP6s or MA104-GCaMP6s-P2Y1ko cells were mock-inoculated or rotavirus-infected with the recombinant SA11cl3-mRuby3 reporter virus and live time-lapse imaging was performed. GCaMP5G reports cytoplasmic Ca^{2+} as changes in fluorescence intensity (green) and rotavirus protein synthesis is reported by mRuby3 expression (pink) from the nonstructural protein 3 (NSP3) open-reading frame. Note the imbedded timer displays time from the beginning of acquisition not the time post-infection.

Supplementary Video 9. CRISPR/Cas9 knockout of the P2Y1 receptor inhibits intercellular calcium waves in human intestinal enteroids.
Jejunum HIE-GCaMP6s, jHIE-GCaMP6s-P2Y1ko, and jHIE-GCaMP6s-P2Y2ko monolayers were mock- or rotavirus (strain Ito)-infected, imaged once per minute for ~7-22 hpi. GCaMP6s reports cytoplasmic Ca^{2+} as changes in fluorescence intensity (green). Note the imbedded timer displays time from the beginning of acquisition not the time post-infection.

Supplementary Video 10. Blocking the P2Y1 receptor decreases RV-induced human intestinal enteroid swelling.
3D jejunum HIE-GCaMP6s enteroids were mock- or rotavirus (strain Ito)-infected, treated with vehicle (DMSO) or 10 μM BPTU, and imaged once per 2-3 min in GFP and differential interference contrast on a widefield epifluorescence microscope for ~3-21 hpi. GCaMP6s reports cytoplasmic Ca^{2+} as changes in fluorescence intensity (green). Note the imbedded timer displays time from the beginning of acquisition not the time post-infection.